

Fluid Flow and Heat Transfer Through an Annular Sector Duct

by

Hamna Afaq



A dissertation submitted in partial fulfillment of the requirements
for the degree of Master of Philosophy in Mathematics

Supervised by

Dr. Mazhar Iqbal

Dr. Asim Aziz

Centre for Advanced Mathematics and Physics

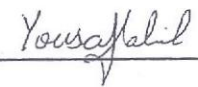
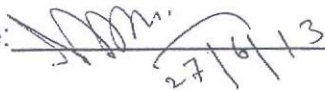


National University of Sciences and Technology

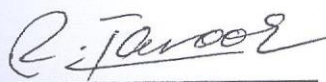
Islamabad, Pakistan

June 2013

National University of Sciences & Technology**M.Phil THESIS WORK**


We hereby recommend that the dissertation prepared under our supervision by: HAMNA AFAQ, Regn No. 2011-NUST-MPHIL PHD-MATHS-27 Titled: Fluid Flow and Heat Transfer Through an Annular Sector Duct be accepted in partial fulfillment of the requirements for the award of **M.Phil** degree.

Examination Committee Members1. Name: Prof. Azad A. SiddiquiSignature: 2. Name: Dr. Yousaf HabibSignature: 3. Name: Dr. M. Muddasar GulzarSignature:  27/6/134. Name: Dr. Rahmat EllahiSignature: 5. Name: Dr. Asim Aziz (Co-Supervisor)Signature: Supervisor's Name: Dr. Mazhar IqbalSignature: 


Head of Department

28/6/2013
Date

COUNTERSIGNEDDate: 28/6/13


Dean/Principal

Fluid Flow and Heat Transfer Through an Annular Sector Duct



by

Hamna Afaq

Centre for Advanced Mathematics and Physics

National University of Sciences and Technology

Islamabad, Pakistan

June 2013

Dedicated
to
My Parents
and
Brothers

Acknowledgements

After praising Allah Almighty who enabled me to conclude my thesis work, I would like to thank my family for all the support they have given me. I would like to extend my gratitude to my professor and supervisor Dr. Mazhar Iqbal for giving me the opportunity to work on this idea and for all the assistance that never ended during the course of this work. It is my pleasure to thank my co-supervisor Dr. Asim for all the assistance and guidance he gave me. I would also like to thank my teachers at CAMP for their guidance during my course work. Finally, I would like to thank all my peers who assisted me whenever I asked them.

Abstract

In this dissertation, fluid flow and heat transfer analysis of fully developed flow through annular sector duct is numerically carried out. The duct consists of two concentric pipes in which hot fluid is flowing in the inner pipe and the cold fluid is flowing through the annulus. The annulus is filled with Darcy-Brinkman's porous media. Longitudinal fins are attached in the annulus in such a way that fins cover full radial width of the annulus. Therefore, the annulus becomes a multi-passage channel in which each passage is an annular sector in shape.

Constant properties incompressible Newtonian fluid is considered. The problem is modeled subject to constant heat flux boundary conditions, H1 condition, applied at the inner surface of the inner pipe. The resulting mathematical model, momentum and energy equations are solved by a fully implicit finite difference method.

The dimensionless bulk mean velocity \hat{w}_m , the product of friction factor with Reynolds number fRe , the dimensionless bulk mean temperature τ_b and the Nusselt number Nu are obtained for clear passage and porous media. The effect of ratio of radii of inner and outer pipe ($\tilde{R} = 0.25, 0.5$), sector angle ($\alpha = 1.047, 0.524, 0.349, 0.262, 0.209, 0.175, 0.15, 0.131$) and permeability ($\hat{K} = 0.001, 0.01, 0.1, 1, 10, 100$) on \hat{w}_m , fRe , τ_b and Nu is observed. The results for the clear passage are verified from the literature. Furthermore, the results are graphically analyzed and conclusions are drawn.

It is seen that the use of porous media enhances heat transfer but friction factor is also increased. Fluid flow and heat transfer can be optimized by maintaining appropriate sector length, sector angle and permeability.

Contents

1	Introduction and Literature Review	1
1.1	Introduction	1
1.2	Literature Review	2
2	Preliminaries	6
2.1	Fluid Flow	6
2.1.1	Steady and Unsteady Flows	6
2.1.2	Laminar and Turbulent Flows	6
2.1.3	Compressible and Incompressible Flow	7
2.1.4	Viscosity	7
2.1.5	Viscous and Inviscid Fluid	7
2.1.6	Newtonian and Non-Newtonian Fluids	8
2.1.7	Velocity Boundary Layer	8
2.1.8	Bulk Mean Velocity	8
2.1.9	Mathematical Model Governing Fluid Flow	9
2.2	Heat Transfer	10
2.2.1	Conduction	10
2.2.2	Convection	11
2.2.3	Radiation	12
2.2.4	Bulk Mean Temperature	12
2.2.5	Generalized Energy Equation	12
2.3	Flow and Heat Transfer Parameters	13
2.3.1	Hydraulic Diameter	13
2.3.2	Reynolds Number	13
2.3.3	Fanning Friction Factor	13

2.3.4	Nusselt Number	14
2.3.5	Prandtl Number	14
2.4	Boundary Conditions	14
2.4.1	Velocity Boundary Condition	14
2.4.2	Thermal Boundary Condition	15
3	Analysis of Fluid Flow Through The Annular Sector	16
3.1	Introduction	16
3.2	Mathematical Modeling	16
3.3	Discretization	19
3.4	Results and Discussion	20
3.5	Validation	29
4	Heat Transfer Through the Annular Sector	31
4.1	Mathematical Model	31
4.2	Results and Discussion	33
4.3	Validation	43
5	Conclusion and Future Work	45
5.1	Conclusion	45
5.2	Future Work	45

List of Tables

3.1	Effect of permeability on \hat{w}_m and fRe for $\tilde{R} = 0.25$	21
3.2	Effect of permeability on \hat{w}_m and fRe for $\tilde{R} = 0.5$	21
3.3	Effect of sector angle on \hat{w}_m and fRe for $\tilde{R} = 0.25, \hat{K} = 1$	22
3.4	Effect of sector angle on w_m and fRe for $\tilde{R} = 0.5, \hat{K} = 1$	25
3.5	Validation with literature for $\hat{K} = \infty$	30
4.1	Effect of permeability on τ_b and Nu for $\tilde{R} = 0.25, \alpha = 0.524$	34
4.2	Effect of permeability on τ_b and Nu for $\tilde{R} = 0.5, \alpha = 0.524$ with $\tau_{bc}=-0.2609,$ $Nu_c=3.0739$	35
4.3	Effect of sector angle for $\tilde{R} = 0.25, \hat{K} = 0.01$	38
4.4	Effect of sector angle for $\tilde{R} = 0.5, \hat{K} = 0.01$	39
4.5	Validation with literature for $\hat{K} = \infty$	43

List of Figures

3.1	(a) Cross-section of the double pipe (b): Computational domain	17
3.2	Velocity profile for (a): $\hat{K} = 100$ (b): $\hat{K} = 10$ (c): $\hat{K} = 1$ (d): $\hat{K} = 0.1$ (e): $\hat{K} = 0.01$ (f): $\hat{K} = 0.001$	23
3.3	Velocity profile for (a): $\hat{K} = 100$ (b): $\hat{K} = 10$ (c): $\hat{K} = 1$ (d): $\hat{K} = 0.1$ (e): $\hat{K} = 0.01$ (f): $\hat{K} = 0.001$	24
3.6	fRe_p values for (a): $\tilde{R} = 0.25$ (b): $\tilde{R} = 0.5$	25
3.4	Velocity profile (a): $\alpha = 1.047$ (b): $\alpha = 0.524$ (c): $\alpha = 0.349$ (d): $\alpha = 0.262$ (e): $\alpha = 0.209$ (f): $\alpha = 0.175$ (g): $\alpha = 0.15$ (h): $\alpha = 0.131$	26
3.5	Velocity profile (a): $\alpha = 1.047$ (b): $\alpha = 0.524$ (c): $\alpha = 0.349$ (d): $\alpha = 0.262$ (e): $\alpha = 0.209$ (f): $\alpha = 0.175$ (g): $\alpha = 0.15$ (h): $\alpha = 0.131$	27
3.7	\hat{w}_{mp} values for (a): $\tilde{R} = 0.25$ (b): $\tilde{R} = 0.5$	28
3.8	Effect of permeability on velocity profile for $\alpha = 0.524$, (a): $\tilde{R} = 0.25$ (b): $\tilde{R} = 0.5$	29
3.9	Effect of permeability on velocity profile for $\alpha = 0.524$, $R = 0.75$, (a): $\tilde{R} = 0.25$ (b): $\tilde{R} = 0.5$	29
4.1	Temperature profile for $\tilde{R} = 0.25$, $\alpha = 0.524$ and (a): $\hat{K} = 100$ (b): $\hat{K} = 10$ (c): $\hat{K} = 1$ (d): $\hat{K} = 0.1$ (e): $\hat{K} = 0.01$ (f): $\hat{K} = 0.001$	36
4.2	Temperature profile for $\tilde{R} = 0.5$, $\alpha = 0.524$ and (a): $\hat{K} = 100$ (b): $\hat{K} = 10$ (c): $\hat{K} = 1$ (d): $\hat{K} = 0.1$ (e): $\hat{K} = 0.01$ (f): $\hat{K} = 0.001$	37
4.5	Nu_p values for (a): $\tilde{R} = 0.25$ (b): $\tilde{R} = 0.5$	39
4.3	Temperature profile for $\tilde{R} = 0.25$, $\hat{K} = 0.01$ and (a): $\alpha = 1.047$ (b): $\alpha = 0.524$ (c): $\alpha = 0.349$ (d): $\alpha = 0.262$ (e): $\alpha = 0.209$ (f): $\alpha = 0.175$ (g): $\alpha = 0.15$ (h): $\alpha = 0.131$	40

4.4	Temperature profile for $\tilde{R} = 0.5$, $\hat{K} = 0.01$ and (a): $\alpha = 1.047$ (b): $\alpha = 0.524$ (c): $\alpha = 0.349$ (d): $\alpha = 0.262$ (e): $\alpha = 0.209$ (f): $\alpha = 0.175$ (g): $\alpha = 0.15$ (h): $\alpha = 0.131$	41
4.6	τ_{bp} values for (a): $\tilde{R} = 0.25$ (b): $\tilde{R} = 0.5$	42
4.7	Effect of permeability on temperature profile for (a): $\tilde{R} = 0.25$ (b): $\tilde{R} = 0.5$. . .	42
4.8	Effect of permeability on temperature profile for $\alpha = 0.524$, $R = 0.75$, (a): $\tilde{R} = 0.25$ (b): $\tilde{R} = 0.5$	43

Chapter 1

Introduction and Literature Review

1.1 Introduction

The concept of boundary layer has central importance in the study of convective heat and mass transfer between surface and the fluid flowing over it. The velocity boundary layer is formed by the the presence of velocity gradients and shear stresses while the thermal boundary layer is due to temperature gradients and heat transfer [1]. The process of heat exchange, which occur due to the difference in temperature between two fluids, has always been given a great importance. A heat exchanger is a device built for efficient heat transfer from one medium to another. The two media can be in direct contact or can be separated by a solid wall. Heat exchangers are useful in almost every industry. For example, space heating, refrigeration, air conditioning, power production, chemical plants, prochemical plants, petroleum refineries, natural gas processing and waste heat recovery etc. In early times parallel plate channels and cylindrical heat exchangers were used. With the passing time, the need of more efficient heat exchangers increased and the researchers came up with the different geometrical designs for heat exchangers such as circular and polygonal tubes.

In the present study, a heat exchanger consisting of two concentric pipes is modeled. Heated fluid is flowing through the inner pipe whereas, the fluid to be heated is flowing through the annulus. Longitudinal fins are attached in the annulus extending from the inner pipe to the outer pipe and the annulus is filled with porous medium in order to enhance the heat transfer. The plan of dissertation is as follows: Chapter 2 consists of fundamental concepts of fluid dynamics and heat transfer. In chapter 3, the fluid flow model is discussed in detail. Momentum equation is solved to get the velocity profile. The bulk mean velocity and fRe are calculated and

the effect of sector length, sector angle and permeability on these parameters is studied. Chapter 4 includes a detailed study of heat transfer model. Bulk mean temperature and Nusselt number is calculated and the effect of sector length, sector angle and permeability on these quantities is discussed. In chapter 5, the research work is concluded and the directions are given for which further research can be done.

1.2 Literature Review

Fluid flow and heat transfer through ducts has been studied by many researchers. Syed et al. [2] studied hydrodynamically fully developed flow and convective heat transfer in the thermal entrance region of finned double-pipe subjected to uniform heat flux thermal boundary condition. They used marching procedure based on finite difference method and computed the numerical solutions of momentum and energy equations. They concluded that the average Nusselt number and the thermal entrance length depends non-monotonically on the ratio of radii, the number of fins and the fin height which indicates that there exist certain values of these parameters for which the total heat transfer within the entry region is maximum. Wang and Tao [3] studied developing steady laminar and constant-property forced-convection flow and heat transfer in annular sector ducts in the entrance region and solved momentum and energy equations numerically using a general marching procedure with both T1 and H1 boundary conditions. They computed Nusselt number and friction factor. Results show that the hydrodynamic entrance length and the thermal entrance length decrease with the increase in sector angle and the ratio of diameters of inner and outer pipe. Moreover the thermal boundary layer develops more rapidly than the hydrodynamic boundary layer. Li et al. [4] studied the fully developed turbulent flow in annular sector ducts. They used mixing length theory, $k - \varepsilon$ model and Reynolds stress model with five apex angles (18, 20, 24, 30, 40°), four radius ratios (2,3,4,5) and Reynolds number range $10^4 - 10^5$. They concluded that none of the turbulence model predict well the fully developed friction factor and the mixing length theory gives best results for the fully developed heat transfer. Syed et al. [5] optimized configuration of annulus in a double pipe with trapezoidal fins augmented to the outer surface of the inner pipe with a fully developed steady, laminar and incompressible flow. They used finite element method for the numerical solution where parameters are number of fins, fin height, fin thickness and the ratio of radii of inner and outer pipes. Constant heat flux condition is imposed and the inner pipe is made up of highly conductive material. Results show that when no parameter is

specified, optimal Nusselt number is obtained when smaller number of shorter and thinner fins augmented to the outer surface of an inner pipe of as smaller a radius as possible.

Researchers have also probed the problem of fluid flow and heat transfer through channels filled with porous medium. Kaviany [6], studied laminar flow through a porous channel bounded by two parallel plates maintained at a constant and equal temperature. The modified Darcy model for transport of momentum is applied but the velocity square term in the momentum equation and the axial conduction term in the energy equation are neglected. The results show that the Nusselt number for fully-developed fields increases with an increase in the porous media shape parameter, $\gamma = \sqrt{W^2 \varepsilon / K}$, where W is channel width, ε is porosity and K is permeability. Sung et al. [7], studied forced convection from an isolated heat source in a channel with porous medium. They calculated ratio of thermal conductivities, Reynolds number, Re and Darcy number, Da and studied their variations. They concluded that as the thickness of the porous substrate, S increases, the flow rate through the opening between the porous layer and the channel wall is increased. A decrease of Da for certain value of S also causes an increase of flow rate, while the flow rate through the porous layer is decreased. For the case when the porous block is attached to the upper surface wall vertically above the heating zone, a decrease of Da results in a decrease of maximum local temperature. For the case when the porous block is connected to the heating zone on the bottom surface wall, however, maximum local temperature increases as Da decreases. It was evident that supportable or unsupported conditions for heat transfer exist according to the changes in S as well as in the geometric arrangement. Kurtbas and Celik [8] investigated the forced and mixed convection heat transfer in a different metallic foam-filled horizontal rectangular channel. They calculated the average and local Nusselt numbers as functions of Reynolds and the Richardson numbers. The results showed that the average Nusselt number increases proportional to pore density and the number increases rapidly with respect to a critic value of Reynolds number. In the region with foam heat transfer increases due to fin effect of foam and the foam behaves as a turbulator. Hooman et al. [9] studied heat transfer and entropy generation optimization. They proposed analytical solutions for temperature distribution and the Nusselt number that envelop three different boundary conditions (all heated, one insulated and two insulated sides cases). They solved the problem numerically and compared the results. They concluded that if the porous media shape parameter $s < 10$ then the best heat transfer rate is achieved in the case when the sides along the width are heated and other are insulated. When $s > 10$ best results are

achieved in the case when one side is insulated. Wang [10] studied fully developed laminar forced convection in a semi-circular channel filled with a Brinkman-Darcy porous medium. He obtained analytical solutions for flow and constant flux heat transfer using a mixture of cartesian and cylindrical coordinates. The problem depends on a parameter s , which is proportional to the inverse square of the Darcy number. He determined friction factor-Reynolds number product and Nusselt number. He concluded that for small s , the velocity profile is rounded similar to the case without the porous medium while for large s , the profile becomes blunted, and a boundary layer exists near the walls. Wang [11] studied the fully developed flow and H1 heat transfer through a polygonal duct filled with a Brinkman-Darcy porous medium. He used boundary collocation method. The non-dimensional parameter used is s which characterizes the inverse square root of permeability. He used The point match method and concluded results for triangular, square and circular ducts and compared with published results. Poulikakos and Kazmierczak [12] studied fully developed forced convection in parallel plates and circular pipe partially filled with a porous material considering both the cases, constant wall heat flux and constant wall temperature. The results show that impact of the parameters (thickness of the porous region adjacent to the wall, the Darcy number and the ratio of the effective thermal conductivity of the porous medium to the fluid thermal conductivity on the heat and fluid flow characteristics of the channel) are similar qualitatively for both channel geometries and boundary conditions. The Nusselt number dependence on the thickness of the porous region is not monotonic. A critical value of the porous region thickness exists at which the Nusselt number value reaches a minimum. Nakayama et al. [13] studied forced convection in a channel filled with a Brinkman-Darcy porous medium the uniform wall heat flux boundary condition. The Brinkman-extended Darcy model is employed to study the effect of the boundary viscous frictional drag on hydrodynamic and heat transfer characteristics. An exact expression is derived for the Nusselt number and approximate results are obtained by exploiting a momentum integral relation. Results show that the approximate formula agree with the exact solution. Hajipour and Dehkordi [14] studied nano-fluid heat transfer in parallel-plate vertical channels partially filled with porous medium. The Brinkmane-Forchheimer extended Darcy model is used. With constant wall temperature, velocity and temperature profiles and expressions for the Nusselt number values are obtained for fully-developed fluid flow. The results show that presence of nano-particles in the base fluid causes a noticeable increase in the velocity and the temperature. Jiang et al. [15] studied forced convection heat transfer of air in plate channels

filled with glass or non-sintered steel spherical particles. They studied the thermal dispersion, variable properties caused by the pressure variation, particle diameter, particle thermal conductivity and the fluid velocity. The experimental results and numerically calculated values for the friction factor in porous media agree with the literature results. The non-sintered porous media increased the heat transfer coefficients. Sheikh and Vafai [16] studied flow and heat transfer in porous media and found the temperature solutions in channels having different cross sectional geometries (parallel plate channel and circular duct). They modified Graetz problem and numerically solved the Brinkmans model. They used another numerical based on the method of weighted residuals. They concluded that the new numerical method improves numerical accuracy. Du et al. [17] conjugated heat transfer in metal foam filled double-pipe. They used two equation numerical model. They concluded that the distributions of excess temperature depend on the relative variation of thermal resistance of inner and annular space in the conjugated heat transfer process.

So far to the knowledge of this author no area has been done on the fluid flow and heat transfer analysis of annular sector duct filled with porous medium.

Chapter 2

Preliminaries

This chapter contains some fundamental concepts. An introduction to fluid flow, different types of fluid flows, the governing equations for the fluid flow and heat transfer are discussed in this chapter. Furthermore, an introduction to heat transfer, the modes of heat transfer and some useful dimensionless quantities are discussed.

2.1 Fluid Flow

A fluid is any substance that deforms continuously when subjected to a shear or tangential stress, no matter how small the stress may be. In other words fluid is something that is capable of flowing and conforms to the shape of containing vessel. Fluids include liquids and gases [18].

2.1.1 Steady and Unsteady Flows

The flow is said to be steady, if all properties of the flow are independent of time i.e.

$$\frac{\partial \lambda}{\partial t} = 0 \quad (2.1)$$

where $\partial/\partial t$ is a derivative with respect to time and λ represents any fluid property. Otherwise, the flow is said to be unsteady or transient flow [18].

2.1.2 Laminar and Turbulent Flows

The flow in which the trajectories followed by fluid particles are regular and smooth and does not change their directions is known as laminar flow. Whereas the flow in which the fluid particles change directions continuously is called a turbulent flow [18].

2.1.3 Compressible and Incompressible Flow

A flow is said to be incompressible if the density of the fluid within the flow is considered to be constant, otherwise the flow is said to be compressible. The mathematical representation of incompressibility of the fluid is given by

$$\frac{D\rho}{Dt} = 0 \quad (2.2)$$

where ρ is density of the fluid and D/Dt is the material time derivative given by

$$\frac{D}{Dt} = \frac{\partial}{\partial t} + \mathbf{V} \cdot \nabla \quad (2.3)$$

In equation (2.3), \mathbf{V} represents the velocity of the flow and ∇ is differential operator. In cartesian coordinate system ∇ is given by

$$\nabla = \frac{\partial}{\partial x} \hat{i} + \frac{\partial}{\partial y} \hat{j} + \frac{\partial}{\partial z} \hat{k} \quad (2.4)$$

where $(\hat{i}, \hat{j}, \hat{k})$ are the unit vectors in their respective directions. In cylindrical coordinate system ∇ is given by

$$\nabla = \frac{\partial}{\partial r} \mathbf{e}_r + \frac{1}{r} \frac{\partial}{\partial \theta} \mathbf{e}_\theta + \frac{\partial}{\partial z} \mathbf{e}_z \quad (2.5)$$

where $(\mathbf{e}_r, \mathbf{e}_\theta, \mathbf{e}_z)$ are the unit vectors in (r, θ, z) directions.

2.1.4 Viscosity

Viscosity is that fluid property by virtue of which a fluid offers resistance to shear stresses. Viscosity of the fluid is measured by the coefficient of viscosity, μ , which is the constant of proportionality between the rate of shear and the tangential force per unit area when parallel plane layers of fluid slide over one another.

2.1.5 Viscous and Inviscid Fluid

A fluid is known as viscous fluid, if it possesses a finite viscosity. While if the dynamic viscosity (a resistance to the flow between layers of a fluid flowing at a given speed) of a fluid is zero than it is said to be inviscid fluid. In general, viscosity of a fluid is never zero but for the experimental purpose in some cases, low values of viscosities can be neglected [18].

2.1.6 Newtonian and Non-Newtonian Fluids

Newtonian fluids obey Newtonian law of viscosity. This means, a fluid in which the shear stress is linearly proportional to the velocity gradient is called a Newtonian fluid. Mathematically, we can write

$$\tau = \mu \frac{\partial \mathbf{v}}{\partial \mathbf{y}} \quad (2.6)$$

where μ is the coefficient of viscosity. While a fluid whose flow properties differ in any respect from those of Newtonian fluids is known as non-Newtonian fluid. In non-Newtonian fluids stress versus strain rate curve is not linear. The expression that describes the fluid behavior is given by

$$\tau = k \left(\frac{\partial u}{\partial y} \right)^n \quad (2.7)$$

where k is the *consistency index* (the measure of the consistency of the fluid) and n is the *flow behavior index* (a measure of how the fluid deviates from the Newtonian fluid). If $n = 1$, then the fluid is Newtonian, otherwise non-Newtonian [18].

2.1.7 Velocity Boundary Layer

When fluid particles interact with a surface, they exhibit a zero velocity. These fluid particles decrease the velocity of next layer of the fluid particles which decreases the velocity of fluid particles of the layer flowing over it. This process goes on until at a certain distance from the flat surface, this retardation effect becomes negligible. Thus, a region is developed in the fluid through which the velocity varies from zero at the surface to some finite value, affiliated with the flow. This region of the fluid is called the hydrodynamics or velocity boundary layer [1].

2.1.8 Bulk Mean Velocity

As the velocity varies over a cross-section during the fluid flow, some unique value of velocity is needed for the calculations. In order to do so, the bulk mean velocity is used when dealing with internal flows which is a very useful quantity. The bulk mean velocity is defined in such a way that it gives mass flow rate \dot{m} , through a tube when it is multiplied by the fluid density ρ and cross-sectional area of the tube A_c . The mass flow rate \dot{m} is defined as [1].

$$\dot{m} = \rho u_m A_c \quad (2.8)$$

where u_m is the bulk mean velocity which is defined as

$$u_m = \frac{1}{A_c} \int \int u r \, dr d\theta \quad (2.9)$$

2.1.9 Mathematical Model Governing Fluid Flow

In this section, we will discuss the generalized mathematical models that govern the fluid flow. These equations are derived on the basis of two fundamental laws: Law of conservation of mass and Law of conservation of momentum.

Generalized Continuity Equation

Continuity equation is based upon Law of conservation of mass which states, "The rate of mass entering and leaving the system is the same". The differential form of continuity equation is given as [19]

$$\frac{\partial \rho}{\partial t} + \nabla \cdot (\rho \mathbf{V}) = 0 \quad (2.10)$$

where \mathbf{V} represents the velocity of the flow and ∇ is differential operator given in equation (2.4).

Generalized Momentum Equations

The momentum equations are the generalized form of *Law of conservation of momentum*, which is derived from Newton's second law of motion. Mathematical form of this law, commonly known as Navier-Stokes equations is given by [19]

$$\rho \frac{Du}{Dt} = -\frac{\partial P}{\partial x} + \frac{\partial \tau_{xx}}{\partial x} + \frac{\partial \tau_{yx}}{\partial y} + \frac{\partial \tau_{zx}}{\partial z} + \rho f_x \quad (2.11)$$

$$\rho \frac{Dv}{Dt} = -\frac{\partial P}{\partial y} + \frac{\partial \tau_{xy}}{\partial x} + \frac{\partial \tau_{yy}}{\partial y} + \frac{\partial \tau_{zy}}{\partial z} + \rho f_y \quad (2.12)$$

$$\rho \frac{Dw}{Dt} = -\frac{\partial P}{\partial z} + \frac{\partial \tau_{xz}}{\partial x} + \frac{\partial \tau_{yz}}{\partial y} + \frac{\partial \tau_{zz}}{\partial z} + \rho f_z \quad (2.13)$$

In equations (2.11)-(2.13) f_x , f_y and f_z are body forces in x , y and z directions respectively, P is the pressure applied on the fluid and τ is the stress tensor whose components are given by Stokes for Newtonian fluids as [19]

$$\tau_{xx} = \lambda(\nabla \cdot \mathbf{V}) + 2\mu \frac{\partial u}{\partial x} \quad (2.14)$$

$$\tau_{yy} = \lambda(\nabla \cdot \mathbf{V}) + 2\mu \frac{\partial v}{\partial y} \quad (2.15)$$

$$\tau_{zz} = \lambda(\nabla \cdot \mathbf{V}) + 2\mu \frac{\partial w}{\partial z} \quad (2.16)$$

$$\tau_{xy} = \tau_{yx} = \mu \left(\frac{\partial v}{\partial x} + \frac{\partial u}{\partial y} \right) \quad (2.17)$$

$$\tau_{xz} = \tau_{zx} = \mu \left(\frac{\partial w}{\partial x} + \frac{\partial u}{\partial z} \right) \quad (2.18)$$

$$\tau_{yz} = \tau_{zy} = \mu \left(\frac{\partial w}{\partial y} + \frac{\partial v}{\partial z} \right) \quad (2.19)$$

In equations (2.14)-(2.19) μ is molecular viscosity and λ is the second viscosity coefficient. According to Stokes

$$\lambda = -\frac{2}{3}\mu \quad (2.20)$$

The vector form of the momentum equations for the Newtonian fluid are given by

$$\rho \left(\frac{\partial \mathbf{V}}{\partial t} + \mathbf{V} \cdot \nabla \mathbf{V} \right) = -\nabla P + \mu \nabla^2 \mathbf{V} + \mathbf{f} \quad (2.21)$$

where \mathbf{V} is velocity of the fluid and ∇ is differential operator.

2.2 Heat Transfer

Heat transfer is the process of the transport of thermal energy due to the spatial temperature difference. The role of heat transfer is to provide the thermodynamic analysis (which consider only the systems in equilibrium), with additional laws that predict the rates of energy transfer [1].

There are three different kinds or processes of heat transfer known as modes of heat transfer i.e. *conduction*, *convection* and *radiation*.

2.2.1 Conduction

Conduction refers to an atomic and molecular heat exchange. It is the transfer of energy (in this case heat energy) from more aggressive to less aggressive particles of a substance due to interaction between particles.

Heat transfer processes can be estimated in terms of rate equations which can be used to compute the amount of energy being transferred per unit time. The rate equation for conduction is referred as the Fourier's law which for one-dimensional plane wall with temperature distribution $T(x)$, is expressed as [1]

$$q_x'' = -\kappa \frac{dT}{dx} \quad (2.22)$$

where q_x'' is the heat flux (W/m^2), κ is the thermal conductivity ($W/m.K$) (characteristic of the wall material which tells how quickly the thermal energy diffuses through the medium). The minus sign shows that heat transfer has occurred in the direction of decreasing temperature.

2.2.2 Convection

The convection heat transfer mode consists of two mechanisms. Because of the molecules on the whole retain their random motion, the total convection happens due to a superposition of energy transport by the random motion of the molecules (diffusion) and by the bulk or microscopic motion of the fluid [1].

Convection heat transfer occurs between a fluid in motion and a bounding surface when the two are at different temperatures due to the formation of velocity boundary layer (described in 2.1.7) and thermal boundary layer (formed whenever there is a temperature difference between the surface and the fluid flowing over that surface. The fluid particles in contact with the surface, achieve equilibrium at the surface's temperature and exchange heat energy with the next layer and so on. In this way, temperature gradients are developed in the fluid. Thus, the area of the fluid containing these temperature gradients is known to be the thermal boundary layer [1].

Since the convection heat transfer mode is due to both the random molecular motion and the bulk motion of the fluid, the contribution due to random molecular motion is more near the surface where the fluid velocity is low. In fact at the interface between the surface and the fluid, the fluid velocity is zero and heat is transferred only by diffusion. The boundary layer grows as the flow progresses in the flow direction and there the heat transfer is due to the bulk fluid motion. As a result, the heat that is conducted into this layer is passed over and is ultimately transferred to the fluid outside the boundary layer.

Classification of convective heat transfer is based upon the nature of the flow. If the flow is caused by external means, it's called *forced convection*. For example by a fan, a pump or atmospheric winds. While in *free (Natural) convection heat transfer*, the transport of heat is not due to some external force but only by density differences in the fluid occurring due to the temperature gradients. For example, hot balloon rising and the chimney effect.

Convection may also occur due to *latent heat exchange*. This latent heat exchange is generally affiliate with a phase change between the liquid and vapor states of the fluid. This may include processes of boiling and condensation.

Regardless of the particular nature of the convection heat transfer process the rate equation representing the process, termed as *Newton's law of cooling*, will be [1]

$$q'' = h(T_s - T_\infty) \quad (2.23)$$

where q'' , the convective heat flux (W/m^2), T_s and T_∞ are the surface and fluid temperatures respectively whereas h ($W/m^2.K$) is the convection heat transfer coefficient. It depends on the boundary layer conditions which depend upon the surface geometry, the nature of the fluid motion and selection of fluid thermodynamic and transport properties.

2.2.3 Radiation

The energy emitted by the matter at non-zero temperature is known as Radiation [1]. The process of radiation can be seen in both solids and fluids. The energy emitted during the process of radiation is transported by electromagnetic waves. Unlike conduction and convection, radiation does not require any material medium. It is more effective in a vacuum. In the present study we have only considered the forced convection.

2.2.4 Bulk Mean Temperature

Like velocity, temperature also varies over a cross-section during the fluid flow and heat transfer process. So we need some mean temperature for the calculation purpose. This bulk mean temperature T_b , is defined as

$$T_b = \frac{1}{u_m A_c} \int \int u T r \, dr d\theta \quad (2.24)$$

where u_m is the bulk mean velocity, T is temperature of the fluid and A_c is cross-sectional area of the tube.

2.2.5 Generalized Energy Equation

Energy equation is the generalized form of *The first law of thermodynamics* according to which the rate of change of energy inside fluid element is equals the sum of net flux of heat into element and rate of work done on the element due to body and surface forces. The non-conservation form of energy equation is given by [19]

$$\begin{aligned} \rho \frac{D}{Dt} \left(e + \frac{V^2}{2} \right) = & \rho \dot{q} + \frac{\partial}{\partial x} \left(k \frac{\partial T}{\partial x} \right) + \frac{\partial}{\partial y} \left(k \frac{\partial T}{\partial y} \right) + \frac{\partial}{\partial z} \left(k \frac{\partial T}{\partial z} \right) \\ & - \frac{\partial up}{\partial x} - \frac{\partial vp}{\partial y} - \frac{\partial wp}{\partial z} + \frac{\partial u\tau_{xx}}{\partial x} + \frac{\partial u\tau_{yx}}{\partial y} + \frac{\partial u\tau_{zx}}{\partial z} + \frac{\partial v\tau_{xy}}{\partial x} + \frac{\partial v\tau_{yy}}{\partial y} \\ & + \frac{\partial v\tau_{zy}}{\partial z} + \frac{\partial w\tau_{xz}}{\partial x} + \frac{\partial w\tau_{yz}}{\partial y} + \frac{\partial w\tau_{zz}}{\partial z} + \rho \mathbf{f} \cdot \mathbf{V} \end{aligned} \quad (2.25)$$

where T is the temperature, ρ is density of the fluid and components of the stress tensor, τ in equation (2.25) are given by equations (2.14)-(2.19).

2.3 Flow and Heat Transfer Parameters

Few important flow and heat transfer parameters which will help to understand the work in the upcoming chapters, are described in this section.

2.3.1 Hydraulic Diameter

The hydraulic diameter is used as the characteristic length of ducts of any shape. It's a ratio between cross-sectional flow area and wetted perimeter [1].

$$D_h = 4 \frac{\text{cross-sectional flow area}}{\text{wetted perimeter}} = 4 \frac{A_c}{p_w}$$

2.3.2 Reynolds Number

Reynolds number Re is a dimensionless number which is the ratio of inertia to viscous forces. A small Reynolds number represents that the inertia forces are a lesser than that of viscous forces resulting a laminar flow. A large Reynolds number however shows the inertia forces are greater than that of viscous forces resulting disturbances resulting into a turbulent flow.

The Reynolds number is represented by the ratio [1]

$$Re = \frac{u_m D_h}{\nu}$$

where u_m is the bulk velocity and $\nu = \mu/\rho$

2.3.3 Fanning Friction Factor

Fanning friction factor is commonly used in fluid flow calculations. It is related to the shear stress at wall. The Fanning friction factor is defined as [1]

$$f = \frac{\tau_s}{\rho u_m^2 / 2}$$

where τ is the stress at wall, defined by,

$$\tau_s = -\mu \left(\frac{du}{dr} \right)_{r=r_o}$$

The product of Fanning friction factor and Reynolds number is commonly used for calculating the friction in a fluid flow. This product is given by,

$$f Re = -\frac{1}{2} \frac{1}{\mu} \frac{dP}{dz} \frac{D_h^2}{u_m}$$

2.3.4 Nusselt Number

The Nusselt number, Nu , is a dimensionless parameter which is the ratio of convection to pure conduction heat transfer. Convective heat transfer is due to the mass motion in the fluid while conduction is due to the particle motion. The increase in Nusselt number means convective heat transfer is relatively more than conductive heat transfer. The increase in Nusselt number show the increase in heat transfer. The Nusselt number is defined as [1]:

$$Nu = \frac{hL}{K_f} = \frac{\partial T^*}{\partial y^*}|_{y^*=0}$$

It can be noted that Nusselt number is actually equal to the dimensionless temperature gradient at the surface and it measures the amount of convective heat transfer at the surface.

2.3.5 Prandtl Number

Prandtl number Pr is a ratio of the momentum to the thermal diffusivity (the thermal conductivity divided by density and specific heat capacity at constant pressure). It roughly estimates either conduction or convection is dominating during the flow. It is defined as [1]:

$$Pr = \frac{c_p \mu}{K} = \frac{\nu}{\alpha}$$

2.4 Boundary Conditions

Boundary conditions play an important role to determine a mathematical solution of a physical problem. A few boundary conditions are given below.

2.4.1 Velocity Boundary Condition

When an inviscid fluid comes in contact with a rigid stationary obstacle during the flow then the normal fluid velocity at the surface of the obstacle must be zero. But in general, the tangential component of the velocity is not zero. In reality, all physical fluids are viscous. Moreover, when a viscous fluid comes in contact with a rigid stationary obstacle during the flow both the normal and the tangential components of the fluid velocity are found to be zero at the obstacles surface. The condition that vertical as well as tangential component of the fluid velocity is zero at a rigid stationary boundary is known as no slip condition.

2.4.2 Thermal Boundary Condition

H1 condition includes constant axial heat flux per unit length of the duct with constant peripheral temperature of the heated wall. This condition suggests that infinite conductivity of heated wall in the radial and transverse directions with zero conductivity in the axial direction [20]. Whereas T1 condition includes constant axial temperature of the duct with constant peripheral temperature of the heated wall. This condition has the same implications for conductivity of the heated wall as in H1 condition [20].

Chapter 3

Analysis of Fluid Flow Through The Annular Sector

3.1 Introduction

The study of fluid flow models is quite important in the area of heat exchangers. Different geometric structures for the fluid flow models are being examined but circular pipes are oftenly used for this purpose. In this chapter the fluid flow in a heat exchanger consisting of two concentric pipes joined by a number of longitudinal fins extending between the inner and outer pipe is modeled and simulated. Heated fluid is flowing through the inner pipe, while the fluid to be heated is flowing through the annulus. Furthermore the annulus is filled with the porous media which may lead the increase in friction and decrease in velocity of the fluid. The bulk mean velocity and fRe are calculated for the flow and the effects of sector length, sector angle and permeability of the fluid are discussed. Results are presented in tabular form as well as graphically.

3.2 Mathematical Modeling

The system consists of two concentric pipe joined by longitudinal fins extending from the inner pipe to the outer (shown in figure (3.1a)). The radius of inner pipe is r_i and that of outer pipe is r_o and the angle between two consecutive fins is 2α . Because of geometric symmetry, we choose half of the region between two consecutive fins as our computational domain as shown in figure (3.1b). So, the resulting sector angle is α and the sector length is $r_o - r_i$. Heated fluid is flowing through the inner pipe while the fluid under consideration is flowing through the outer

pipe with velocity (u,v,w) in a concurrent manner.

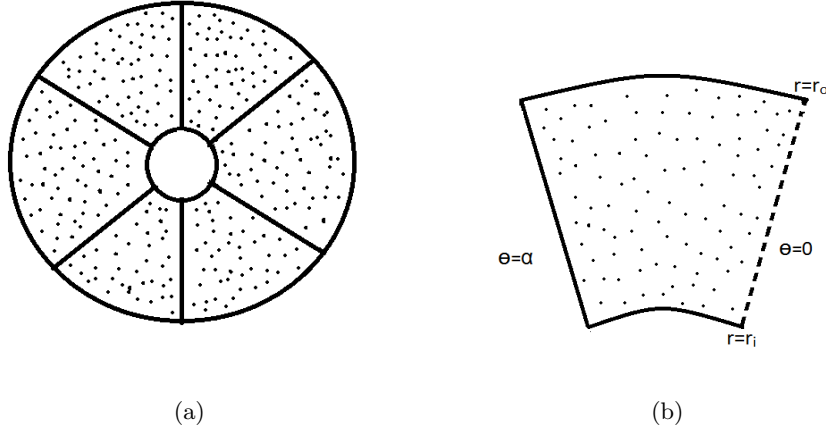


Figure 3.1: (a) Cross-section of the double pipe (b): Computational domain

The fluid flowing through the annulus is considered to be viscous, incompressible, Newtonian and with constant properties. The flow is assumed to be steady, laminar and hydrodynamically fully-developed. All body forces and viscous dissipations are neglected. The only driving force is constant pressure gradient in axial direction. The governing model for the fluid flow in cylindrical polar co-ordinates can be written as,

Continuity equation (in cylindrical polar co-ordinates):

$$\frac{\partial P}{\partial t} + \frac{1}{r} \frac{\partial(r\rho u)}{\partial r} + \frac{1}{r} \frac{\partial\rho v}{\partial\theta} + \frac{\partial\rho w}{\partial z} = 0 \quad (3.1)$$

Navier-Stokes equations (in cylindrical polar co-ordinates):

$$\rho \left(\frac{\partial u}{\partial t} + u \frac{\partial u}{\partial r} + \frac{v}{r} \frac{\partial u}{\partial\theta} + w \frac{\partial u}{\partial z} - \frac{v^2}{r} \right) = -\frac{\partial P}{\partial r} + \mu \left[\frac{1}{r} \frac{\partial}{\partial r} \left(r \frac{\partial u}{\partial r} \right) + \frac{1}{r^2} \frac{\partial^2 u}{\partial\theta^2} \right] + \mu \left[\frac{\partial^2 u}{\partial z^2} - \frac{u}{r^2} - \frac{2}{r^2} \frac{\partial v}{\partial\theta} \right] + \rho g_r \quad (3.2)$$

$$\rho \left(\frac{\partial v}{\partial t} + u \frac{\partial v}{\partial r} + \frac{v}{r} \frac{\partial v}{\partial\theta} + w \frac{\partial v}{\partial z} - \frac{uv}{r} \right) = -\frac{1}{r} \frac{\partial P}{\partial\theta} + \mu \left[\frac{1}{r} \frac{\partial}{\partial r} \left(r \frac{\partial v}{\partial r} \right) + \frac{1}{r^2} \frac{\partial^2 v}{\partial\theta^2} \right] + \mu \left[\frac{\partial^2 v}{\partial z^2} - \frac{v}{r^2} + \frac{2}{r^2} \frac{\partial u}{\partial\theta} \right] + \rho g_\theta \quad (3.3)$$

$$\rho \left(\frac{\partial w}{\partial t} + u \frac{\partial w}{\partial r} + \frac{v}{r} \frac{\partial w}{\partial\theta} + w \frac{\partial w}{\partial z} \right) = -\frac{\partial P}{\partial z} + \mu \left[\frac{1}{r} \frac{\partial}{\partial r} \left(r \frac{\partial w}{\partial r} \right) \right] + \mu \left[\frac{1}{r^2} \frac{\partial^2 w}{\partial\theta^2} + \frac{\partial^2 w}{\partial z^2} \right] + \rho g_z \quad (3.4)$$

where g_r , g_θ and g_z are body forces (gravities) along respective directions. For a porous medium in the sector, according to Darcy-Brinkman model equations (3.2), (3.3) and (3.4) become

$$\rho \left(\frac{\partial u}{\partial t} + u \frac{\partial u}{\partial r} + \frac{v}{r} \frac{\partial u}{\partial \theta} + w \frac{\partial u}{\partial z} - \frac{v^2}{r} \right) = -\frac{\partial P}{\partial r} + \mu \left[\frac{1}{r} \frac{\partial}{\partial r} \left(r \frac{\partial u}{\partial r} \right) \right] + \mu \left[\frac{1}{r^2} \frac{\partial^2 u}{\partial \theta^2} + \frac{\partial^2 u}{\partial z^2} - \frac{u}{r^2} - \frac{2}{r^2} \frac{\partial v}{\partial \theta} + \frac{u}{K} \right] + \rho g_r \quad (3.5)$$

$$\rho \left(\frac{\partial v}{\partial t} + u \frac{\partial v}{\partial r} + \frac{v}{r} \frac{\partial v}{\partial \theta} + w \frac{\partial v}{\partial z} - \frac{uv}{r} \right) = -\frac{1}{r} \frac{\partial P}{\partial \theta} + \mu \left[\frac{1}{r} \frac{\partial}{\partial r} \left(r \frac{\partial v}{\partial r} \right) \right] + \mu \left[\frac{1}{r^2} \frac{\partial^2 v}{\partial \theta^2} + \frac{\partial^2 v}{\partial z^2} - \frac{v}{r^2} + \frac{2}{r^2} \frac{\partial u}{\partial \theta} - \frac{v}{K} \right] + \rho g_\theta \quad (3.6)$$

$$\rho \left(\frac{\partial w}{\partial t} + u \frac{\partial w}{\partial r} + \frac{v}{r} \frac{\partial w}{\partial \theta} + w \frac{\partial w}{\partial z} \right) = -\frac{\partial P}{\partial z} + \mu \left[\frac{1}{r} \frac{\partial}{\partial r} \left(r \frac{\partial w}{\partial r} \right) \right] + \mu \left[\frac{1}{r^2} \frac{\partial^2 w}{\partial \theta^2} + \frac{\partial^2 w}{\partial z^2} - \frac{w}{K} \right] + \rho g_z \quad (3.7)$$

where K is the permeability of the medium.

As the flow is assumed to be steady there will be no time dependent derivative in continuity and momentum equations. The continuity equation for incompressible flow can be written as [19],

$$\frac{1}{r} \frac{\partial(ru)}{\partial r} + \frac{1}{r} \frac{\partial v}{\partial \theta} + \frac{\partial w}{\partial z} = 0 \quad (3.8)$$

The momentum equations (3.5), (3.6) and (3.7) after applying the above mentioned conditions becomes

$$\frac{\partial P}{\partial r} = 0 \quad (3.9)$$

$$\frac{\partial P}{\partial \theta} = 0 \quad (3.10)$$

$$\mu \left[\frac{1}{r} \frac{\partial}{\partial r} \left(r \frac{\partial w}{\partial r} \right) + \frac{1}{r^2} \frac{\partial^2 w}{\partial \theta^2} - \frac{w}{K} \right] - \frac{\partial P}{\partial z} = 0 \quad (3.11)$$

Equation (3.9) and (3.10) shows that there is no pressure gradient along r or θ direction.

Therefore governing equation reduces to

$$\frac{\partial^2 w}{\partial r^2} + \frac{1}{r} \frac{\partial w}{\partial r} + \frac{1}{r^2} \frac{\partial^2 w}{\partial \theta^2} - \frac{w}{K} = \frac{1}{\mu} \frac{\partial P}{\partial z} \quad (3.12)$$

with respect to boundary conditions

$$\text{at } r = r_i, \quad w = 0 \quad (3.13)$$

$$\text{at } r = r_o, \quad w = 0 \quad (3.14)$$

$$\text{at } \theta = 0, \quad \frac{\partial w}{\partial \theta} = 0 \quad (3.15)$$

$$\text{at } \theta = \alpha, \quad w = 0 \quad (3.16)$$

The above equation and boundary conditions are made dimensionless by using following dimensionless quantities

$$R = \frac{r}{r_o}, \quad \hat{w} = \frac{w}{\frac{1}{\mu} r_o^2 \frac{\partial P}{\partial z}} \quad (3.17)$$

$$\tilde{R} = \frac{r_i}{r_o}, \quad \hat{K} = \frac{K}{r_o^2} \quad (3.18)$$

So, the dimensionless form of equation (3.12) can be written as

$$\frac{\partial^2 \hat{w}}{\partial R^2} + \frac{1}{R} \frac{\partial \hat{w}}{\partial R} + \frac{1}{R^2} \frac{\partial^2 \hat{w}}{\partial \theta^2} - \frac{\hat{w}}{\hat{K}} = 1 \quad (3.19)$$

and the boundary conditions become

$$\text{at } R = \tilde{R}, \quad \hat{w} = 0 \quad (3.20)$$

$$\text{at } R = 1, \quad \hat{w} = 0 \quad (3.21)$$

$$\text{at } \theta = 0, \quad \frac{\partial \hat{w}}{\partial \theta} = 0 \quad (3.22)$$

$$\text{at } \theta = \alpha, \quad \hat{w} = 0 \quad (3.23)$$

3.3 Discretization

Second order finite difference approximations are used to discretize the governing equation as under.

$$\frac{\partial^2 w}{\partial R^2} = \frac{w(i+1, j) - 2w(i, j) + w(i-1, j)}{h^2} + O(h^2)$$

$$\frac{\partial^2 w}{\partial \theta^2} = \frac{w(i, j+1) - 2w(i, j) + w(i, j-1)}{k^2} + O(k^2)$$

and

$$\frac{\partial w}{\partial R} = \frac{w(i+1, j) - w(i-1, j)}{2h} + O(h^2)$$

where h is the step size in r -direction and k is step size in θ -direction. By putting these approximations in equation (3.19) and solving for $w(i, j)$, the discretized form of equation

(3.19) becomes

$$\begin{aligned}
w(i, j) = & \frac{h^2 k^2 R(i)^2}{2(R(i)^2 k^2 + h^2)} \left(\frac{1}{h^2} + \frac{1}{2R(i)h} \right) w(i+1, j) \\
& + \frac{h^2 k^2 R(i)^2}{2(R(i)^2 k^2 + h^2)} \left(\frac{1}{h^2} - \frac{1}{2R(i)h} \right) w(i-1, j) + \frac{h^2 (w(i, j+1) - w(i, j-1))}{2(R(i)^2 k^2 + h^2)} \\
& - \frac{h^2 k^2 R(i)^2}{2(R(i)^2 k^2 + h^2)} \frac{u(i-1, j) + u(i+1, j)}{2\hat{K}} + \frac{h^2 k^2 R(i)^2}{2(R(i)^2 k^2 + h^2)} \quad (3.24)
\end{aligned}$$

3.4 Results and Discussion

In this section results pertaining to the flow parameters like velocity profile bulk mean velocity and fRe are presented in tabular as well as in graphical form. For this purpose the discretized equation (3.24) is solved by SOR method. The effect of parameters like \tilde{R} , \hat{K} and α is discussed by varying their values as under:

- $\tilde{R} = 0.25, 0.5$
- $\hat{K} = 0.001, 0.01, 0.1, 1, 10, 100$
- $\alpha = 1.047, 0.524, 0.349, 0.262, 0.209, 0.175, 0.15, 0.131$

In order to study the characteristics of the flow, we find the product of fanning friction factor and the Reynolds number as

$$fRe = \frac{4\alpha^2(1 - \tilde{R}^2)^2}{[\alpha(1 + \tilde{R}) + (1 - \tilde{R})]^2}$$

Tables 3.1-3.2 show the effect of permeability \hat{K} , bulk mean velocity \hat{w}_m and fRe for a given sector angle α and ratio of radii \tilde{R} . Percentage change in both, the mean velocity through porous media \hat{w}_{mp} and the friction factor multiplied with Reynolds number for porous media fRe_p is given corresponding to their values for clear passage ($\hat{K} = \infty$). Table 3.1 shows the effect of permeability on bulk mean velocity and fRe when \tilde{R} , α are taken as 0.25 and 1.047 respectively. The clear passage mean velocity \hat{w}_{mc} and fRe_c in this case are 0.0298 and 15.2530 respectively.

Table 3.1: Effect of permeability on \hat{w}_m and fRe for $\tilde{R} = 0.25$

\hat{K}	\hat{w}_{mp}	% change in \hat{w}_m	fRe_p	% change in fRe
100	0.0298	0.0404	15.2591	0.0404
10	0.0297	0.4029	15.3147	0.4045
1	0.0287	3.8822	15.8690	4.0390
0.1	0.0213	28.5019	21.3334	39.8639
0.01	0.0063	78.7884	71.9087	371.4411
0.001	0.0009	97.0655	519.7828	3307.7512

It can be seen from the table that the bulk mean velocity decreases substantially as \hat{K} decreases from 100 to 0.001. The percentage change in w_m with $\hat{K} = 100$ is only 0.0404 and the change is as high as 97.0655 percent with $\hat{K} = 0.001$. This is due to the retardation of fluid particles as the permeable space is decreased and friction is increased.

The fRe increases as permeability decreases by keeping other parameters constant. This trend is inline with the physics of the problem because the permeable space in the medium is decreased causing the increase in friction. For $\hat{K} = 100$, fRe is 15.5291 and that for $\hat{K} = 0.001$ it is 519.7828 which is 3307.7512 % more than the fRe for clear passage.

Table 3.2 shows the effect of permeability on bulk mean velocity and fRe when $\tilde{R} = 0.5$ whereas α remains same. The \hat{w}_{mc} and fRe_c in this case are 0.0167 and 17.2398 respectively.

Table 3.2: Effect of permeability on \hat{w}_m and fRe for $\tilde{R} = 0.5$

\hat{K}	\hat{w}_{mp}	% change in \hat{w}_m	fRe_p	% change in fRe
100	0.0167	0.0218	17.2436	0.0218
10	0.0167	0.2180	17.2775	0.2185
1	0.0163	2.1367	17.6162	2.1834
0.1	0.0137	17.8254	20.9795	21.6921
0.001	0.0008	94.9670	342.5348	1886.8829

It can be seen that the trend remains same for larger \tilde{R} , however, the numerical values in the case of larger \tilde{R} are relatively small. The sector length decreases as \tilde{R} increases because

$\tilde{R} = r_i/r_o$ and sector length is $r_o - r_i$.

Thus the ratio of the permeable space to the whole space in the sector decreases as \tilde{R} increases causing an increase in friction and retardation. Now we study the effect of change in permeability on the velocity profile. Figures (3.2a) to (3.2f) show the velocity contours for $\tilde{R} = 0.25$ and $\alpha = 1.047$.

It can be seen from the figures (3.2a) to (3.2f) that the velocity gradients increase among the adjacent layers in the fluid as \hat{K} decreases. That is why decreasing permeability decreases the bulk velocity and increases the fRe . We can observe that the maximum velocity region also increases with decreasing permeability enhancing the fluid flow.

We see the same pattern when we change ratio of radii by keeping other parameters constant. This trend can be observed in figures (3.3a) to (3.3f).

Now we study the effect of sector angle by keeping other parameters constant. The effect of change of sector angle on \hat{w}_m and fRe is shown in table 3.3, which shows the values for $\hat{K} = 1$ and $\tilde{R} = 0.25$.

Table 3.3: Effect of sector angle on \hat{w}_m and fRe for $\tilde{R} = 0.25$, $\hat{K} = 1$

α	\hat{w}_{mp}	\hat{w}_{mc}	% change in \hat{w}_m	fRe_p	fRe_c	% change in fRe
1.047	0.0287	0.0298	3.8822	15.8690	15.2530	4.0390
0.524	0.0164	0.0168	2.2489	14.8897	14.5548	2.3007
0.349	0.0101	0.0102	1.3856	15.1133	14.9039	1.4051
0.262	0.0067	0.0068	0.9313	15.4344	15.2907	0.9401
0.209	0.0048	0.0048	0.6685	15.7097	15.6047	0.6730
0.175	0.0036	0.0036	0.5029	15.9322	15.8521	0.5054
0.15	0.0028	0.0028	0.3921	16.1125	16.0493	0.3937
0.131	0.0022	0.0022	0.3142	16.2605	16.2094	0.3152

It can be noted that by varying sector angle, the fRe first decreases and then increases with the decrease in sector angle. This change is due to the fact that the ratio of permeable space to total space of the sector first increases and then goes on decreasing with the decrease in sector angle. Therefore friction first decreases and then increases so the fRe decreases then increases

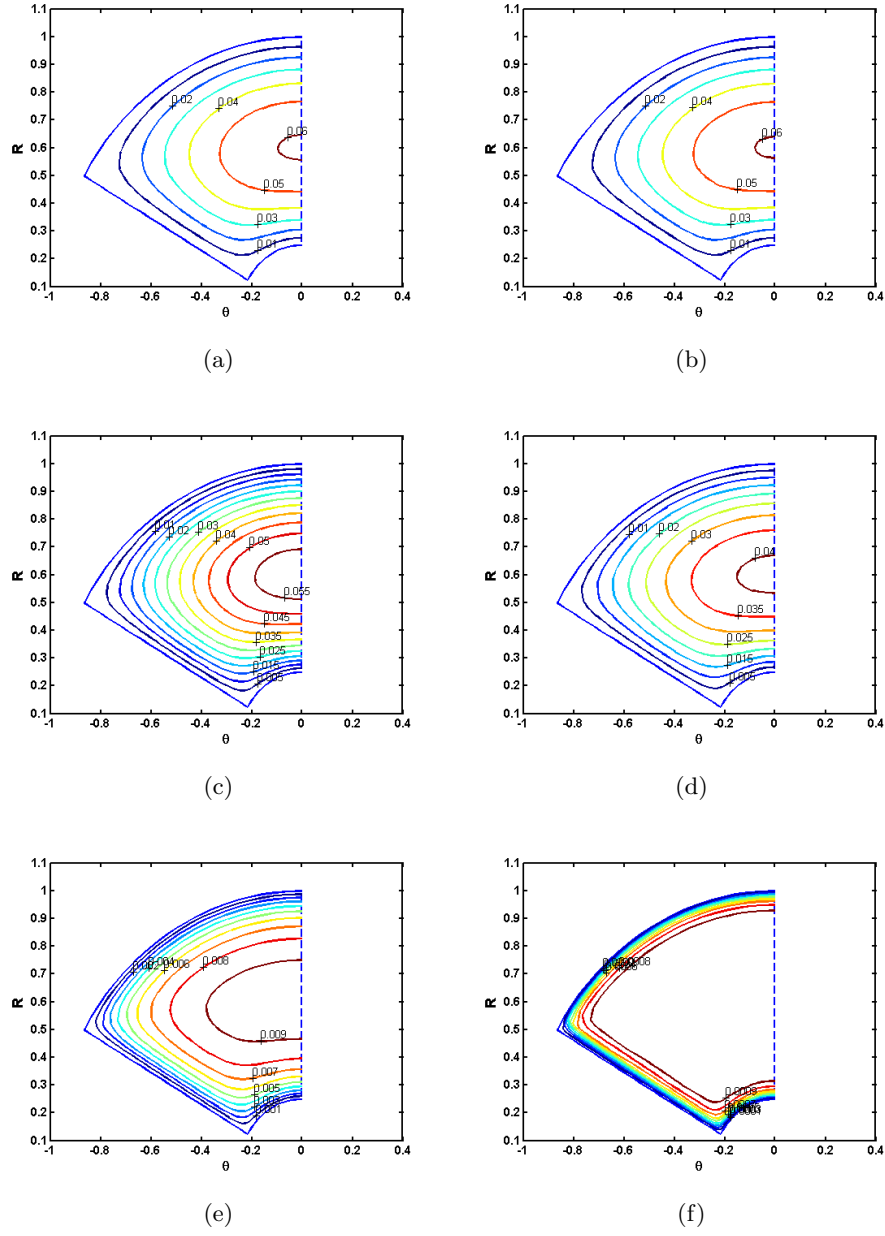


Figure 3.2: Velocity profile for (a): $\hat{K} = 100$ (b): $\hat{K} = 10$ (c): $\hat{K} = 1$ (d): $\hat{K} = 0.1$ (e): $\hat{K} = 0.01$ (f): $\hat{K} = 0.001$

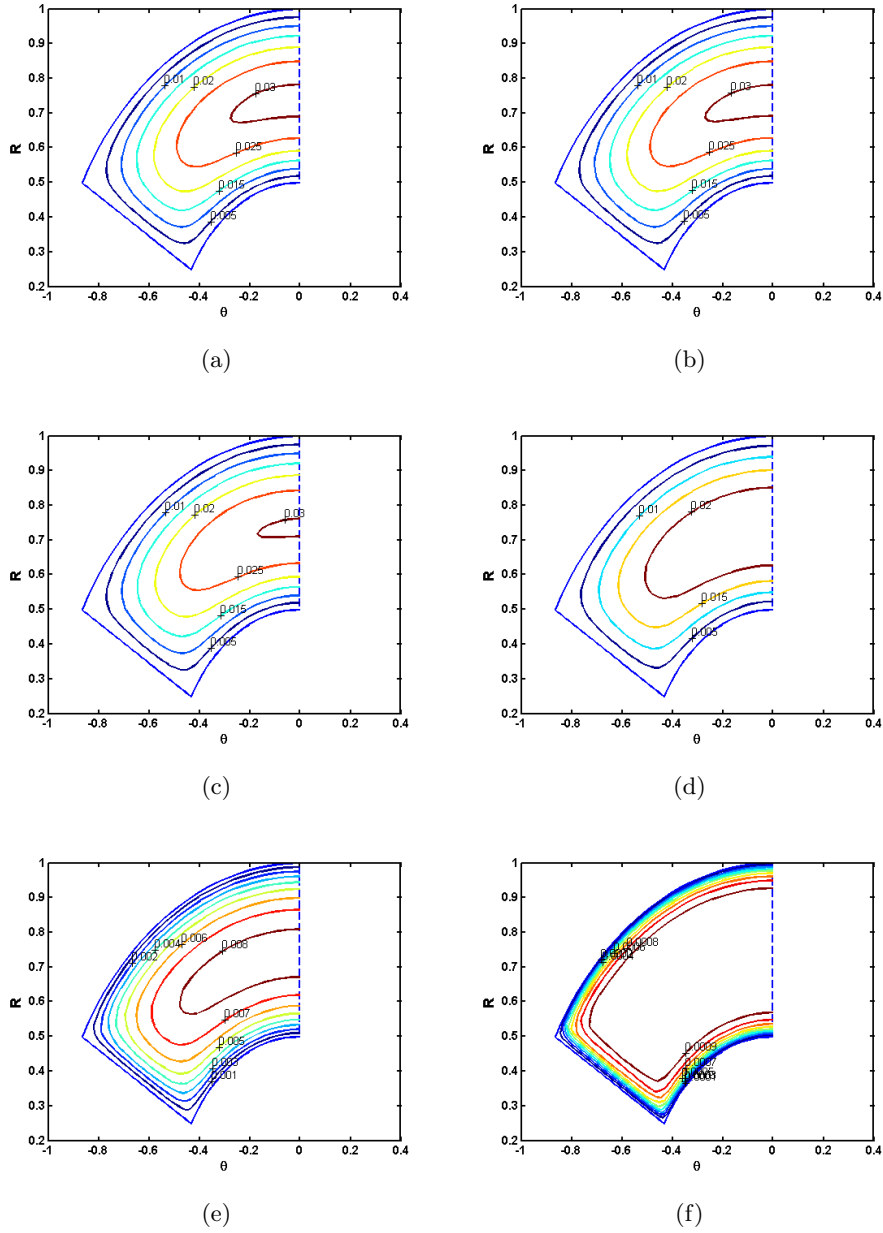


Figure 3.3: Velocity profile for (a): $\hat{K} = 100$ (b): $\hat{K} = 10$ (c): $\hat{K} = 1$ (d): $\hat{K} = 0.1$ (e): $\hat{K} = 0.01$ (f): $\hat{K} = 0.001$

with decreasing sector angle. the velocity decreases as the friction increases with the decrease of sector angle.

If we change \tilde{R} to 0.5 from 0.25 the trend of \hat{w}_m and fRe remains identical. This can be observed from table 3.4.

Table 3.4: Effect of sector angle on w_m and fRe for $\tilde{R} = 0.5$, $\hat{K} = 1$

α	\hat{w}_{mp}	\hat{w}_{mc}	% change in \hat{w}_m	fRe_p	fRe_c	% change in fRe
1.047	0.0163	0.0167	2.1367	17.6162	17.2398	2.1834
0.524	0.0123	0.0125	1.6786	15.1360	14.8820	1.7072
0.349	0.0090	0.0091	1.2383	14.5106	14.3309	1.2538
0.262	0.0066	0.0067	0.9083	14.6082	14.4755	0.9166
0.209	0.0050	0.0050	0.6795	14.9602	14.8585	0.6841
0.175	0.0038	0.0039	0.5220	15.3811	15.3008	0.5247
0.15	0.0030	0.0030	0.4110	15.7990	15.7341	0.4127
0.131	0.0025	0.0025	0.3315	16.1884	16.1347	0.3326

Now we study the effect of sector angle on the velocity profile in figures (3.4a) to (3.5h).

From the figures (3.4a) to (3.5h) we can conclude that the velocity decreases as the friction increases and a boundary layer formation is more clear (that is, velocity gradients between layers of the fluid increases) with the decrease of sector angle. Now we will discuss the fRe_p corresponding to different values of α and \hat{K} figures (3.6a) and (3.6b) show the fRe values for different α and \hat{K} when \tilde{R} is taken to be as 0.25 and 0.5 respectively.

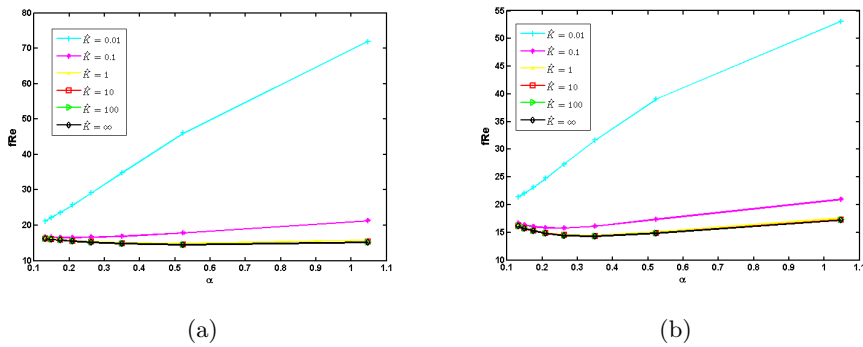


Figure 3.6: fRe_p values for (a): $\tilde{R} = 0.25$ (b): $\tilde{R} = 0.5$

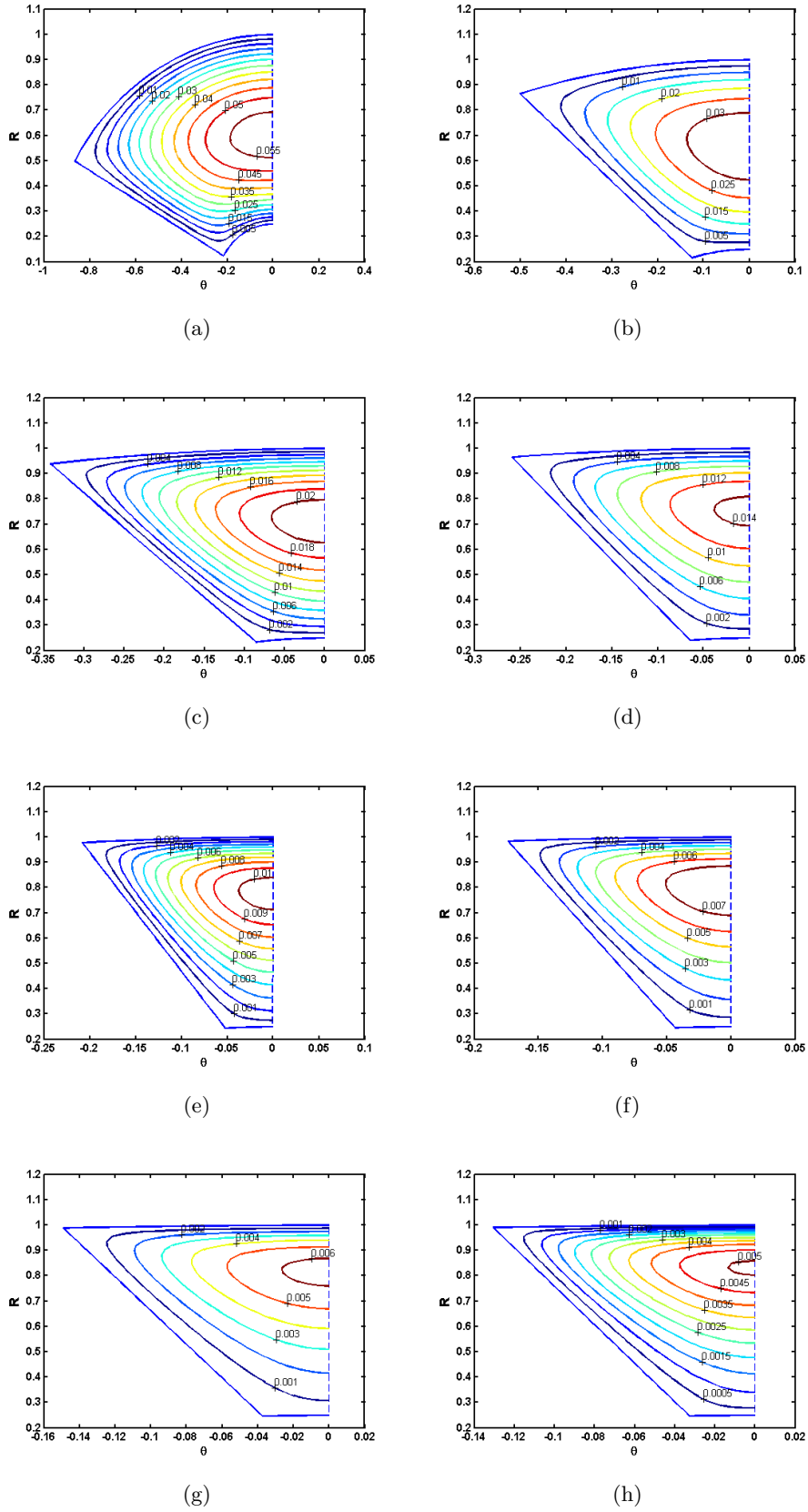


Figure 3.4: Velocity profile (a): $\alpha = 1.047$ (b): $\alpha = 0.524$ (c): $\alpha = 0.349$ (d): $\alpha = 0.262$ (e): $\alpha = 0.209$ (f): $\alpha = 0.175$ (g): $\alpha = 0.15$ (h): $\alpha = 0.131$

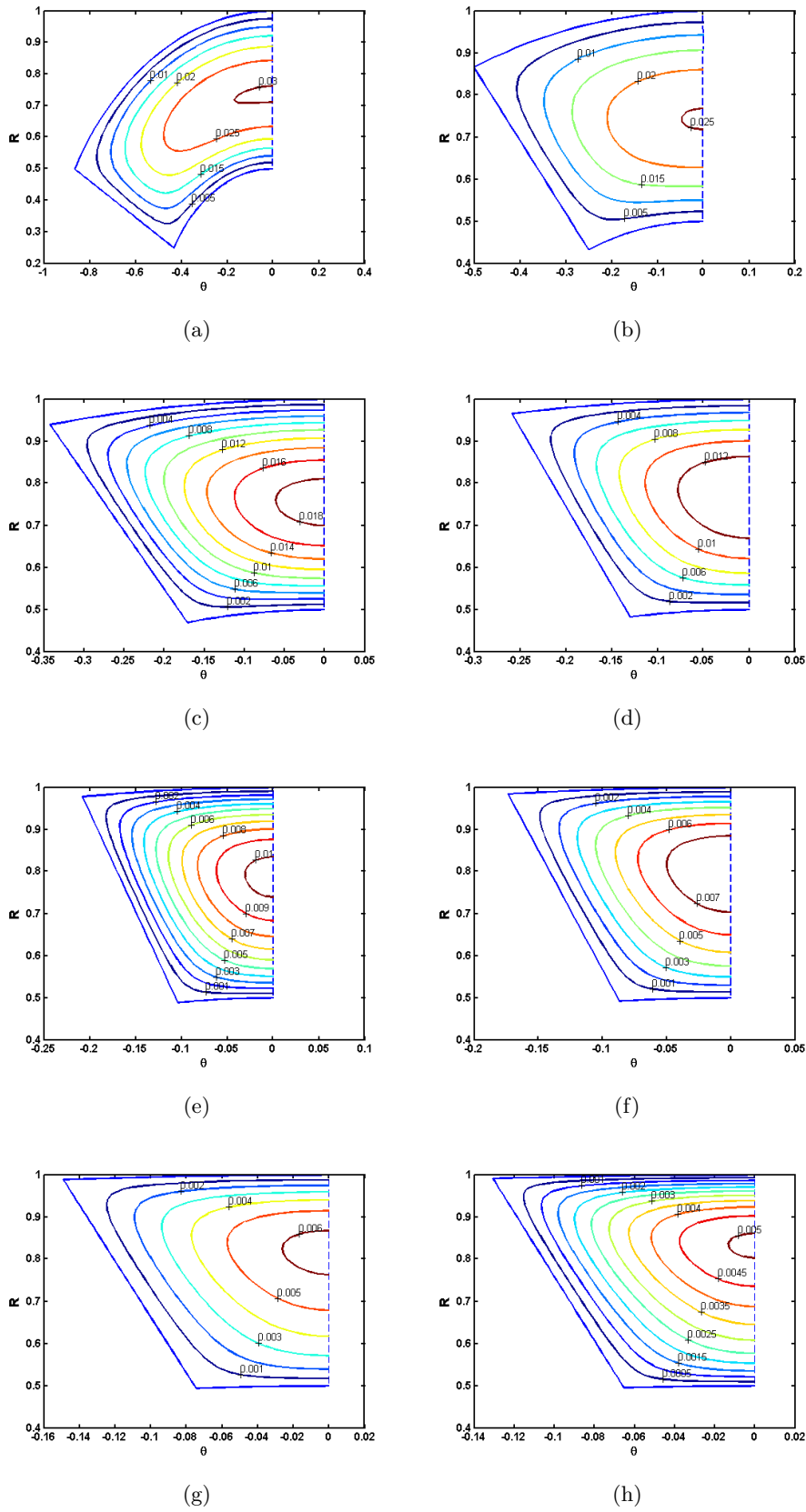


Figure 3.5: Velocity profile (a): $\alpha = 1.047$ (b): $\alpha = 0.524$ (c): $\alpha = 0.349$ (d): $\alpha = 0.262$ (e): $\alpha = 0.209$ (f): $\alpha = 0.175$ (g): $\alpha = 0.15$ (h): $\alpha = 0.131$

It can be seen that for a particular sector angle, by decreasing permeability, fRe increases. While for a particular permeability value less than 0.01, by changing sector angle, fRe increases. But for permeability value greater than 0.01, by changing sector angle, fRe first decreases and then increases. This is due to the fact that the ratio of permeable space to the total space in the fluid for permeability greater than 0.01 first increases with the sector angle and then goes on decreasing causing friction to show this pattern. Comparison of figures (3.6a) and (3.6b) shows that response of fRe_p is invariant to \tilde{R} .

Now we will observe the effect of permeability and sector angle on the bulk velocity.

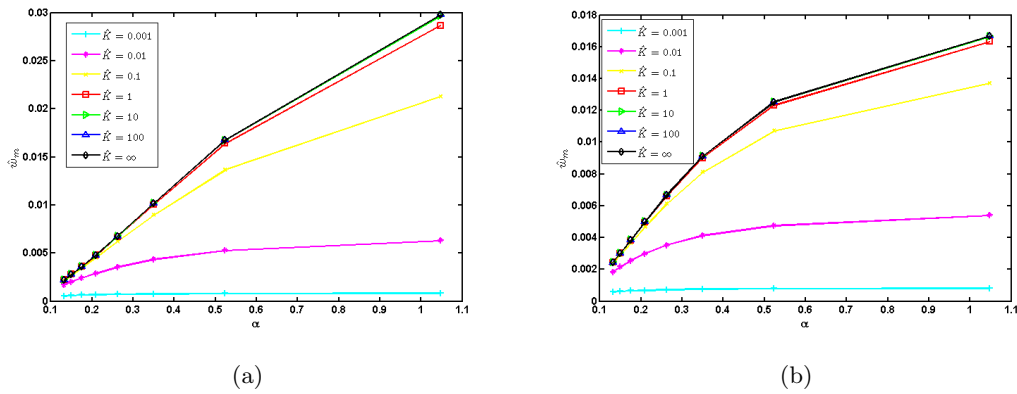


Figure 3.7: \hat{u}_{mp} values for (a): $\tilde{R} = 0.25$ (b): $\tilde{R} = 0.5$

We can easily see in the figures (3.7a) and (3.7b) that for a particular sector angle, by decreasing permeability, u_m decreases. While for a particular permeability, u_m increases with the increase of sector angle.

Now we study the effect of permeability on velocity profile. For this purpose the velocity is plotted for a particular R and θ value. Figures (3.8a) and (3.8b) show the effect of permeability for $\tilde{R} = 0.25$ and $\tilde{R} = 0.5$ respectively for $\theta = 0.2618$ and given α . Whereas figures (3.9a) and (3.9b) show the same effect for $R = 0.75$ and for a given α .

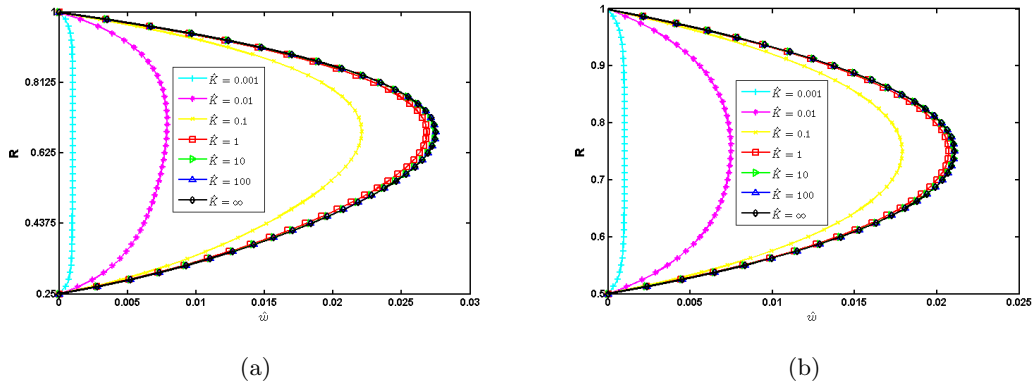


Figure 3.8: Effect of permeability on velocity profile for $\alpha = 0.524$, (a): $\tilde{R} = 0.25$ (b): $\tilde{R} = 0.5$

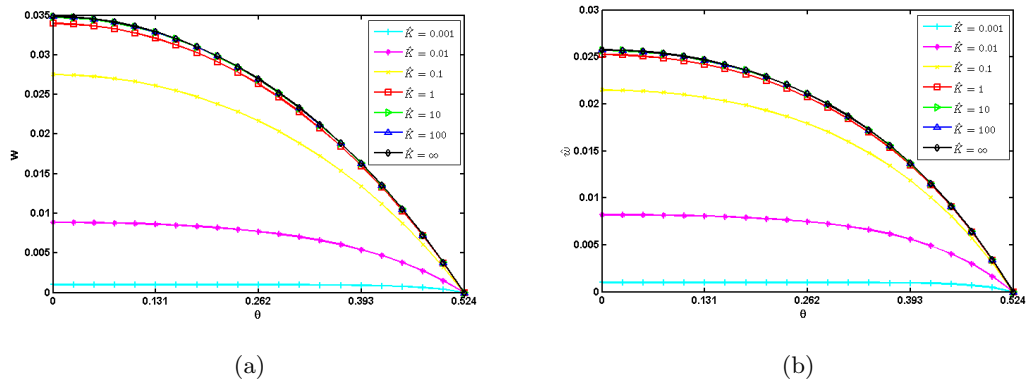


Figure 3.9: Effect of permeability on velocity profile for $\alpha = 0.524$, $R = 0.75$, (a): $\tilde{R} = 0.25$ (b): $\tilde{R} = 0.5$

The figures clearly indicate the retardation in the velocity as the value of \hat{K} is decreased.

3.5 Validation

In this section a comparison of the fRe values calculated in the present study for clear passage with that available in literature [21] are discussed. Table 3.5 show the comparison for $\tilde{R} = 0.25$ and $\tilde{R} = 0.5$ respectively where \hat{K} is considered to be infinity.

Table 3.5: Validation with literature for $\hat{K} = \infty$

\tilde{R}	α	fRe		% change in fRe
		Calculated	Literature	
0.25	0.524	14.5548	14.546	0.06
	0.262	15.2907	15.281	0.063
	0.175	15.8520	15.839	0.082
	0.131	16.2094	16.193	0.1
0.5	0.524	14.8820	14.872	0.067
	0.262	14.4755	14.467	0.059
	0.175	15.3008	15.291	0.064
	0.131	16.1347	16.123	0.073

It can be seen from the tables that percentage change in fRe is within 1% which shows that the procedure adopted in this study is valid and the results obtained are compatible with literature.

Chapter 4

Heat Transfer Through the Annular Sector

Energy in the form of heat is transferred from a system to its surroundings due to temperature difference. The study of the heat transfer has always been of great importance. In this chapter we will model the fully developed heat transfer phenomenon in the same computational domain as discussed in the previous chapter. Results will be presented for the temperature profile, bulk mean temperature and Nusselt number. The effect of sector length, sector angle and permeability will be studied. Moreover, validation of the model will be carried out with the literature results.

4.1 Mathematical Model

In this section we will present the mathematical model of the forced convective heat transfer mechanism through the annular sector. The heat transfer is assumed to be steady and thermally fully developed. The viscous dissipations and axial heat conduction effect in the fluid as well as in solids are neglected. Furthermore the heat transfer surface is considered to be isothermal. The assumptions for the fluid flow are same as discussed in the previous chapter. The problem is modeled subject to constant heat flux boundary conditions known as H1 boundary conditions. The transfer of heat energy through the flowing fluid is calculated by the energy equation which in cylindrical polar co-ordinates is represented as

$$\rho c_p \left(\frac{\partial T}{\partial t} + u \frac{\partial T}{\partial r} + \frac{v}{r} \frac{\partial T}{\partial \theta} + w \frac{\partial T}{\partial z} \right) = \mu \left(\frac{\partial^2 T}{\partial r^2} + \frac{1}{r} \frac{\partial T}{\partial r} + \frac{1}{r^2} \frac{\partial^2 T}{\partial \theta^2} + \frac{\partial^2 T}{\partial z^2} \right) \quad (4.1)$$

According to assumptions the energy equation (4.1) reduces to

$$\frac{\rho c_p}{\mu} w \frac{\partial T}{\partial z} = \frac{\partial^2 T}{\partial r^2} + \frac{1}{r} \frac{\partial T}{\partial r} + \frac{1}{r^2} \frac{\partial^2 T}{\partial \theta^2} \quad (4.2)$$

Taking energy balance over a small element we have

$$\dot{q}' dz = A_c \rho c_p \bar{w} dT_b \quad (4.3)$$

$$\frac{dT_b}{dz} = \frac{\dot{q}'}{A_c \rho c_p \bar{w}} \quad (4.4)$$

where \dot{q}' be the heat transfer rate per unit length. Let τ be a dimensionless quantity defined by

$$\tau = \frac{T - T_w}{\dot{q}'/\lambda_f} \quad (4.5)$$

As the fluid is thermally fully developed, therefore

$$\frac{\partial \tau}{\partial z} = 0 \quad (4.6)$$

this yields

$$\frac{\partial}{\partial z} \left(\frac{T - T_w}{\dot{q}'/\lambda_f} \right) = 0 \quad (4.7)$$

Thus

$$\frac{\partial T}{\partial z} = \frac{\partial T_w}{\partial z} \quad (4.8)$$

also

$$\frac{\partial}{\partial z} \left(\frac{T_b - T_w}{\dot{q}'/\lambda_f} \right) = 0 \quad (4.9)$$

Therefore

$$\frac{\partial T_b}{\partial z} = \frac{\partial T_w}{\partial z} \quad (4.10)$$

Comparing equations (4.4), (4.8) and (4.10) we have

$$\frac{\partial T}{\partial z} = \frac{\dot{q}'}{A_c \rho c_p \bar{w}} \quad (4.11)$$

Equations (4.2) and (4.11) become

$$\frac{\partial^2 T}{\partial r^2} + \frac{1}{r} \frac{\partial T}{\partial r} + \frac{1}{r^2} \frac{\partial^2 T}{\partial \theta^2} = \frac{w}{A_c \bar{w} \lambda} \dot{q}' \quad (4.12)$$

The boundary conditions are

$$\text{at } r = r_i, \quad T = T_w, \quad 0 < \theta < \alpha \quad (4.13)$$

$$\text{at } r = r_o, \quad \frac{\partial T}{\partial r} = 0, \quad 0 < \theta < \alpha \quad (4.14)$$

$$\text{at } \theta = 0, \quad \frac{\partial T}{\partial \theta} = 0, \quad r_i < r < r_o \quad (4.15)$$

$$\text{at } \theta = \alpha, \quad T = T_w, \quad r_i < r < r_o \quad (4.16)$$

In equation (4.5) we have defined a dimensionless quantity τ as

$$\tau = \frac{T - T_w}{\dot{q}'/\lambda_f} \quad (4.17)$$

Using transformations defined in equations (4.5), (3.17) and (3.18), the above model is made dimensionless. The dimensionless form of equation (4.12) is

$$\frac{\partial^2 \tau}{\partial R^2} + \frac{1}{R} \frac{\partial \tau}{\partial R} + \frac{1}{R^2} \frac{\partial^2 \tau}{\partial \theta^2} = \frac{\hat{w}}{A_c \hat{w}^m} \quad (4.18)$$

with respect to boundary conditions

$$\text{at } R = \tilde{R}, \quad \tau = 0, \quad 0 < \theta < \alpha \quad (4.19)$$

$$\text{at } R = 1, \quad \frac{\partial \tau}{\partial r} = 0, \quad 0 < \theta < \alpha \quad (4.20)$$

$$\text{at } \theta = 0, \quad \frac{\partial \tau}{\partial \theta} = 0, \quad \tilde{R} < R < 1 \quad (4.21)$$

$$\text{at } \theta = \alpha, \quad \tau = 0, \quad \tilde{R} < R < 1 \quad (4.22)$$

4.2 Results and Discussion

The equation (4.18) is solved subject to the boundary conditions using the second order finite difference method as the same grid layout as discussed in chapter 4.2. The resulting system of algebraic equation is solved with the help of SOR method. Results are presented for temperature profile, bulk mean temperature and the Nusselt number and in effect of the parameters like \tilde{R} , α and \hat{K} is discussed in both tabular as well as graphical manner. For this purpose we have used same values of these parameters as discussed in chapter 4.2.

The velocity profile required to solve the energy equation (4.12) has already been obtained in chapter . In order to study the characteristics of heat transfer during the flow, we find the average Nusselt number as follows

$$Nu = -\frac{D_h^*}{h_p^* \tau_b} \quad (4.23)$$

where

$$D_h^* = \frac{2\alpha(1 - \tilde{R}^2)}{\alpha(\tilde{R} + 1) + (1 - \tilde{R})}, \quad h_p^* = \alpha\tilde{R} + (1 - \tilde{R}) \quad (4.24)$$

and

$$\tau_b = \frac{\int \int R w \tau dR d\theta}{\int \int R w dR d\theta} \quad (4.25)$$

Table 4.1 show the effect of permeability on the bulk mean temperature τ_{bp} and the Nusselt number Nu_p in porous media for $\tilde{R} = 0.25$ and $\alpha = 0.524$. The corresponding values of τ_{bc} and Nu_c for clear passage are 0.2369 and 3.3493 respectively.

Table 4.1 shows that the Nusselt number increases by a small amount as permeability decreases by keeping other parameters constant. The Nusselt number is the ratio of convective to conductive heat transfer. The increase in Nusselt number means convective heat transfer is relatively more than conductive heat transfer. It can be seen that the bulk temperature increases as permeability decreases due to increase in friction and velocity remains constant which means that the heat transfer is increasing.

Table 4.1: Effect of permeability on τ_b and Nu for $\tilde{R} = 0.25$, $\alpha = 0.524$

\hat{K}	τ_{bp}	% change in τ_b	Nu_p	% change in Nu
100	-0.2369	0.0014	3.3494	0.0014
10	-0.2369	0.0135	3.3498	0.0135
1	-0.2366	0.1343	3.3538	0.1343
0.1	-0.2339	1.2858	3.3924	1.2858
0.01	-0.2171	9.1169	3.6547	9.1169
0.001	-0.1875	26.3368	4.2315	26.3368

The effect of permeability on τ_{bp} and Nu_p for $\tilde{R} = 0.5$ and $\alpha = 0.524$ is shown in table 4.2. The general trend of increase in Nusselt number and bulk mean temperature can also be observed in this table. Therefore, we conclude that altering the value of \tilde{R} does not change the heat transfer pattern.

Table 4.2: Effect of permeability on τ_b and Nu for $\tilde{R} = 0.5$, $\alpha = 0.524$ with $\tau_{bc}=-0.2609$, $Nu_c=3.0739$

\hat{K}	τ_{bp}	% change in τ_b	Nu_p	% change in Nu
100	-0.2609	0.0011	3.0740	0.0011
10	-0.2609	0.0109	3.0743	0.0109
1	-0.2606	0.1079	3.0772	0.1079
0.1	-0.2582	1.0373	3.1058	1.0373
0.01	-0.2425	7.6173	3.3081	7.6173
0.001	-0.2108	23.7800	3.8049	23.78

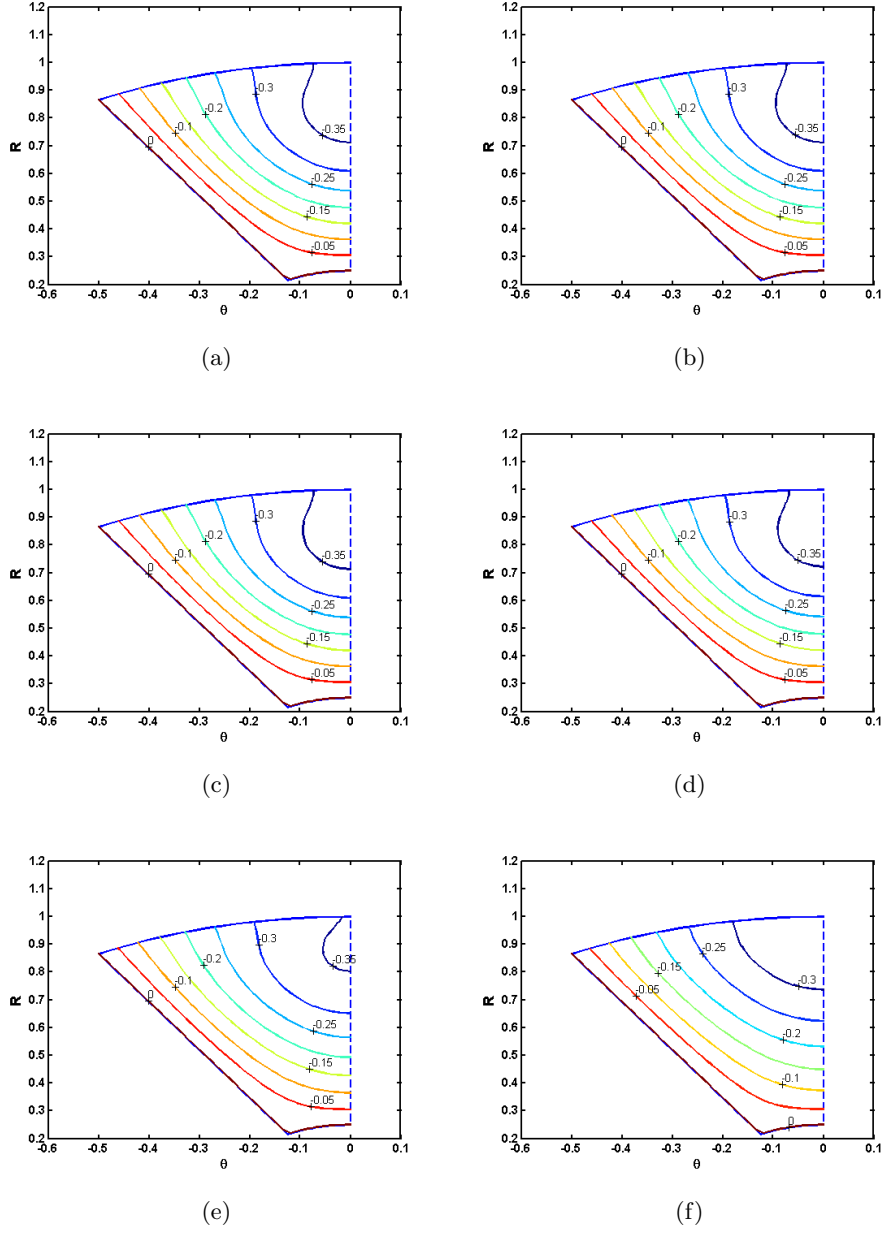


Figure 4.1: Temperature profile for $\tilde{R} = 0.25$, $\alpha = 0.524$ and (a): $\hat{K} = 100$ (b): $\hat{K} = 10$ (c): $\hat{K} = 1$ (d): $\hat{K} = 0.1$ (e): $\hat{K} = 0.01$ (f): $\hat{K} = 0.001$

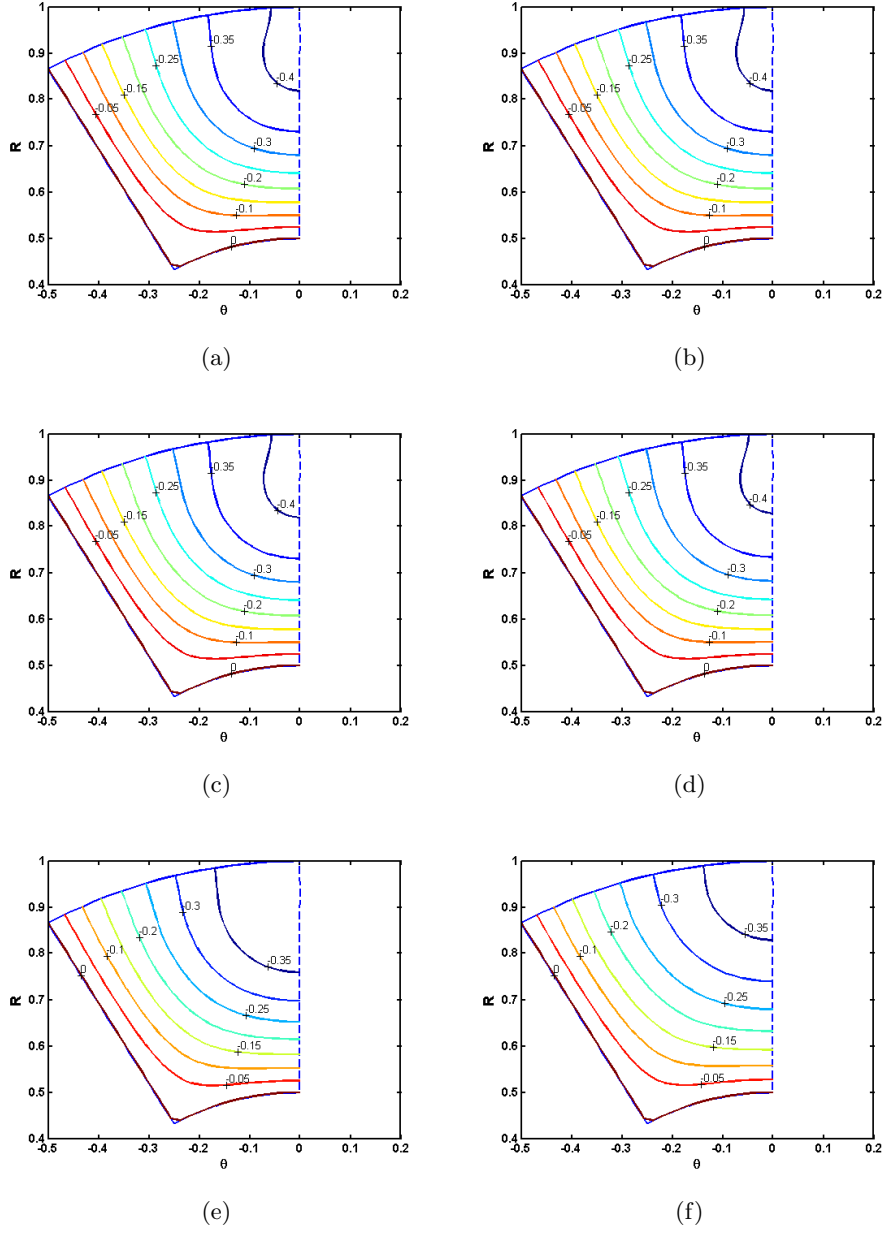


Figure 4.2: Temperature profile for $\tilde{R} = 0.5$, $\alpha = 0.524$ and (a): $\hat{K} = 100$ (b): $\hat{K} = 10$ (c): $\hat{K} = 1$ (d): $\hat{K} = 0.1$ (e): $\hat{K} = 0.01$ (f): $\hat{K} = 0.001$

Figures (4.1a) to (4.2f) show the temperature profile for $\tilde{R} = 0.25$ and $\tilde{R} = 0.5$ respectively. When α is taken to be 0.524. The subfigures show the permeability on the temperature profile. The markings in the figures show the difference of temperature from the heated sides (i.e. the inner pipe and the fin) of the sector. It can be seen that as permeability decreases the temperature difference between heated wall and the fluid at a certain point increases indicating enhancement in heat transfer. The trend remains same for both values of \tilde{R} .

Now we study the effect of sector angle on the bulk mean temperature and the Nusselt number for the given value of permeability. Tables 4.3 and 4.4 show the effect of sector angle when \tilde{R} is taken to be 0.25 and 0.5 respectively. It can be observed that τ_b and Nu has monotonic behavior for $\tilde{R} = 0.25$ whereas this monotonic behavior ceases to exist for $\tilde{R} = 0.5$. This suggests the existence of an optimized geometry for which heat transfer rate is maximum.

Table 4.3: Effect of sector angle for $\tilde{R} = 0.25$, $\hat{K} = 0.01$

α	τ_{bp}	τ_{bc}	% change in τ_b	Nu_p	Nu_c	% change in Nu
1.047	-0.2795	-0.3107	11.1519	3.3722	3.0339	11.1519
0.524	-0.2171	-0.2369	9.1169	3.6547	3.3493	9.1169
0.349	-0.1707	-0.1849	8.3263	3.8606	3.5638	8.3263
0.262	-0.1418	-0.1529	7.8230	3.9407	3.6548	7.823
0.209	-0.1223	-0.1311	7.2209	3.9551	3.6887	7.2209
0.175	-0.1081	-0.1152	6.5570	3.9401	3.6976	6.557
0.15	-0.0972	-0.1029	5.9015	3.9134	3.6953	5.9015
0.131	-0.0884	-0.0931	5.2931	3.8833	3.6881	5.2931

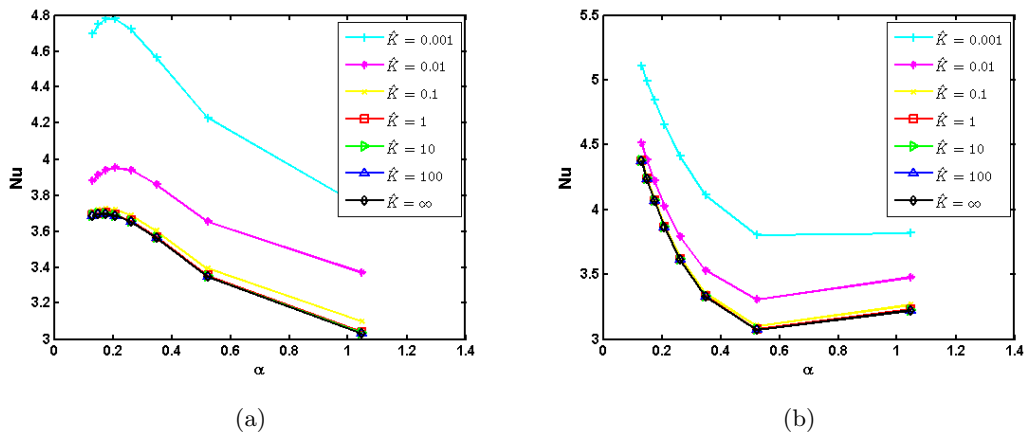
Table 4.4: Effect of sector angle for $\tilde{R} = 0.5$, $\hat{K} = 0.01$

α	τ_{bp}	τ_{bc}	% change in τ_b	Nu_p	Nu_c	% change in Nu
1.047	-0.2129	-0.2297	7.8776	3.4800	3.2259	7.8776
0.524	-0.2425	-0.2609	7.6173	3.3081	3.0739	7.6173
0.349	-0.2147	-0.2276	6.0050	3.5320	3.3319	6.005
0.262	-0.1837	-0.1928	4.9319	3.7953	3.6169	4.9319
0.209	-0.1583	-0.1651	4.2522	4.0298	3.8654	4.2522
0.175	-0.1229	-0.1271	3.4131	4.2252	4.0713	3.7787
0.15	-0.1229	-0.1271	3.4131	4.2252	4.0713	3.7787
0.131	-0.1105	-0.1139	3.1089	4.5143	4.3782	3.1089

Figures (4.3a) to (4.4h) show the effect of sector angle on the temperature profile for $\tilde{R} = 0.25$ and $\tilde{R} = 0.5$ respectively. When \hat{K} is taken to be 0.01.

It can be observed that the colder region decreases with the sector angle. As the sector angle decreases, the value of τ_b decreases for a certain region, i.e., the temperature difference from the wall decreases enhancing the heat transfer. Same pattern is seen for $\tilde{R} = 0.5$.

The graphical representation of the effect of sector angle on Nu_p and τ_{bp} for different values of \hat{K} is given in figures (4.5a) and (4.6b). The figures substantiate the observation of presence of an optimal geometry for which heat transfer rate is maximum.

Figure 4.5: Nu_p values for (a): $\tilde{R} = 0.25$ (b): $\tilde{R} = 0.5$

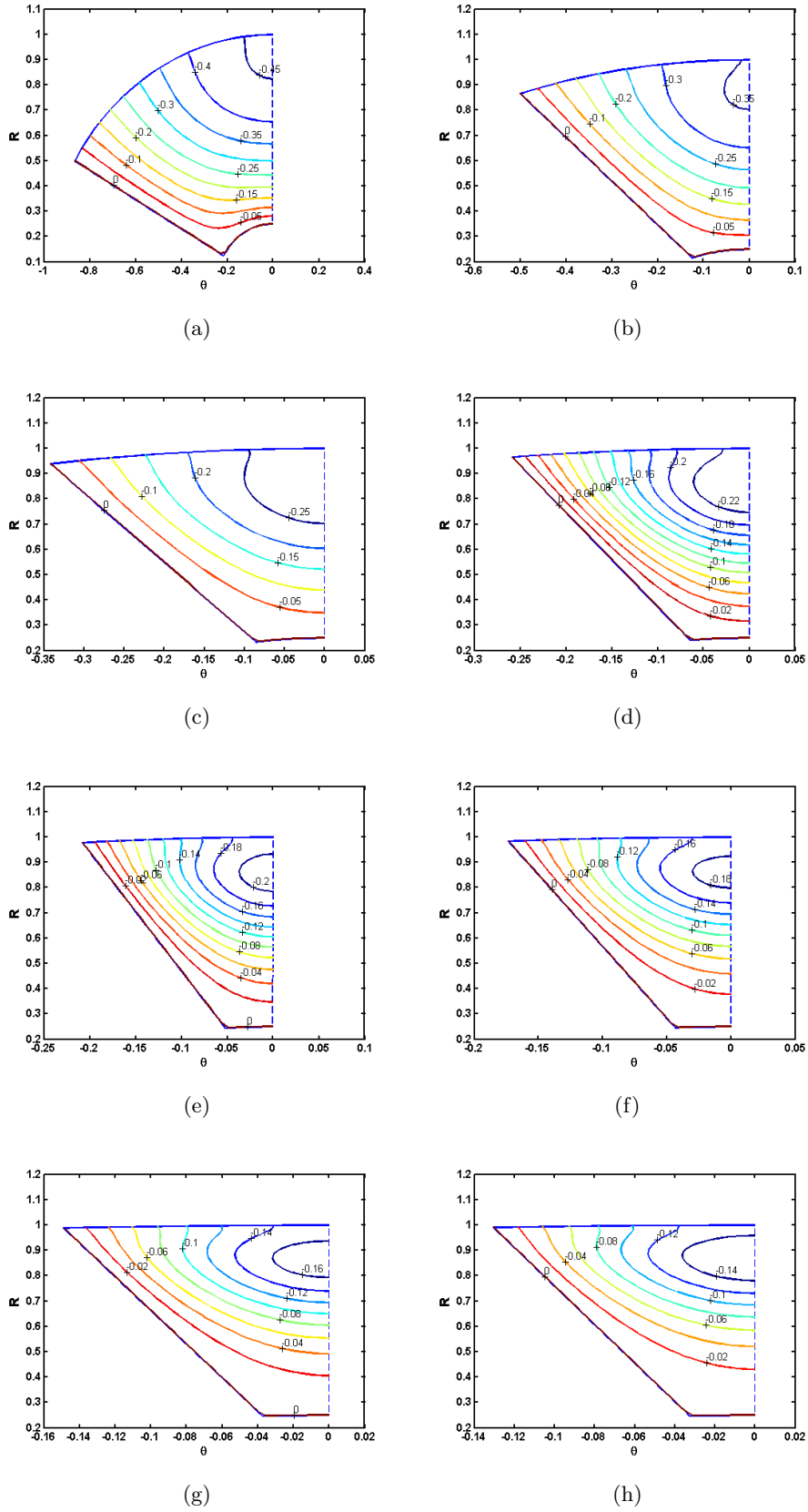


Figure 4.3: Temperature profile for $\tilde{R} = 0.25$, $\hat{K} = 0.01$ and (a): $\alpha = 1.047$ (b): $\alpha = 0.524$ (c): $\alpha = 0.349$ (d): $\alpha = 0.262$ (e): $\alpha = 0.209$ (f): $\alpha = 0.175$ (g): $\alpha = 0.15$ (h): $\alpha = 0.131$

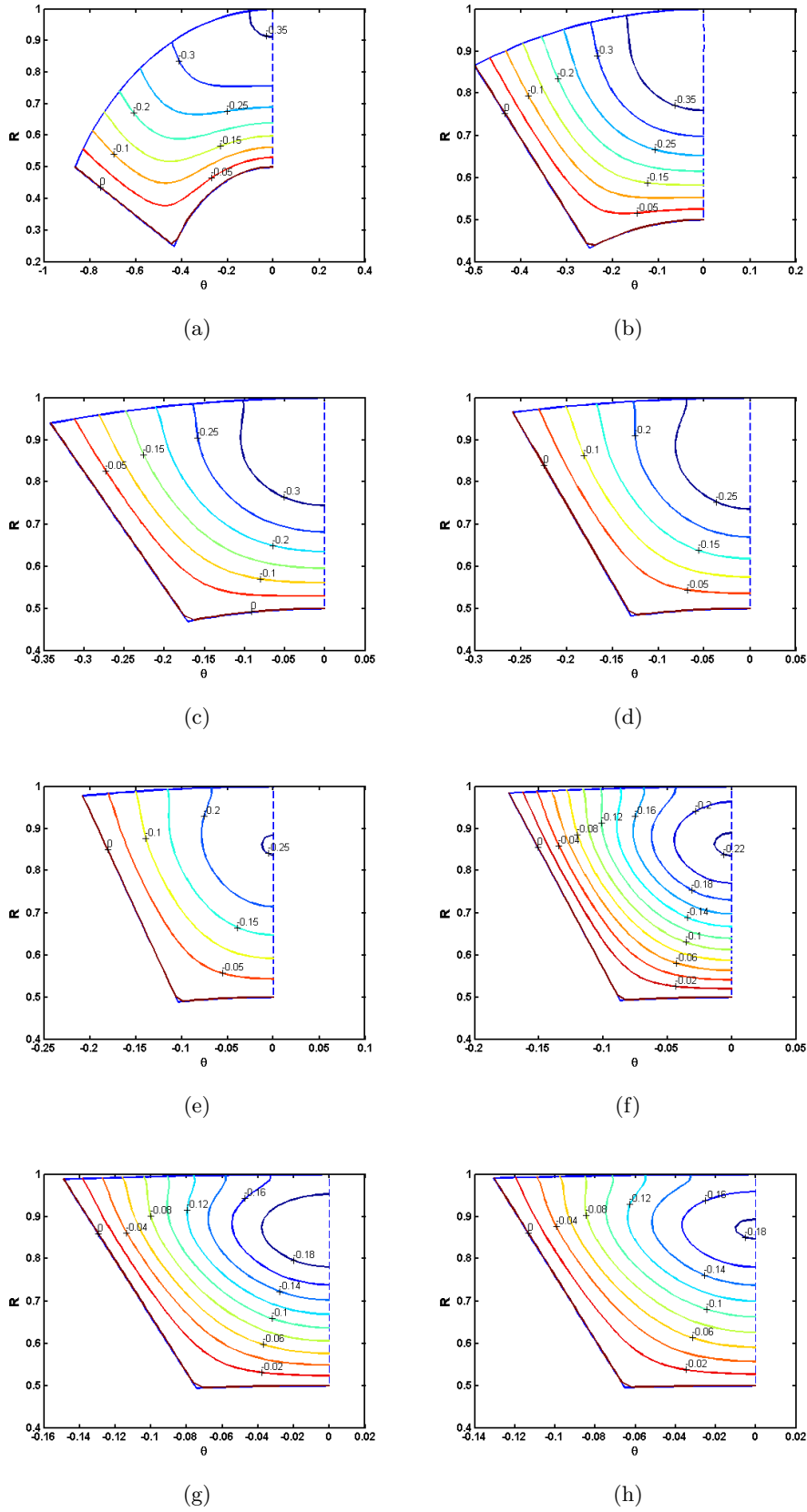


Figure 4.4: Temperature profile for $\tilde{R} = 0.5$, $\hat{K} = 0.01$ and (a): $\alpha = 1.047$ (b): $\alpha = 0.524$ (c): $\alpha = 0.349$ (d): $\alpha = 0.262$ (e): $\alpha = 0.209$ (f): $\alpha = 0.175$ (g): $\alpha = 0.15$ (h): $\alpha = 0.131$

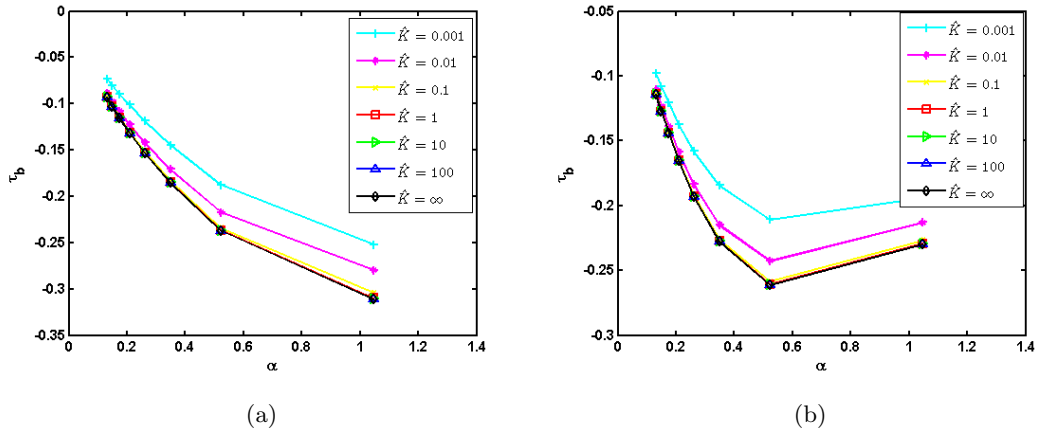


Figure 4.6: τ_{bp} values for (a): $\tilde{R} = 0.25$ (b): $\tilde{R} = 0.5$

Now we see the effect of permeability on the isotherms for a given θ and R values. Figures (4.7a) and (4.7b) show the effect of permeability for $\tilde{R} = 0.25$ and $\tilde{R} = 0.5$ respectively when α is fixed at 0.524 and θ is taken as 0.2618. Whereas figures (4.8a) and (4.8b) show the effect of permeability for $R = 0.75$ whereas the other parametric values kept same.

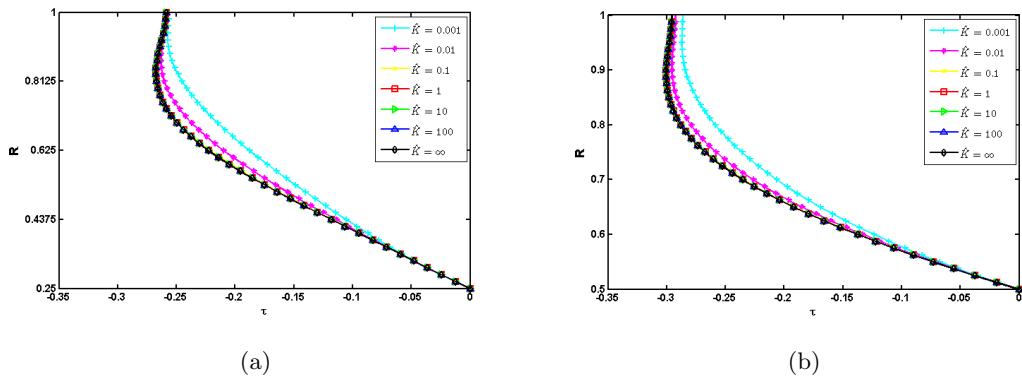


Figure 4.7: Effect of permeability on temperature profile for (a): $\tilde{R} = 0.25$ (b): $\tilde{R} = 0.5$

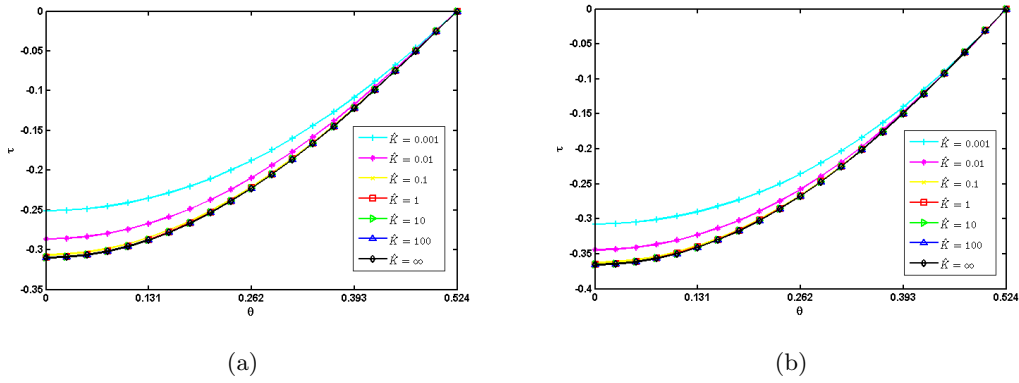


Figure 4.8: Effect of permeability on temperature profile for $\alpha = 0.524$, $R = 0.75$, (a): $\tilde{R} = 0.25$
 (b): $\tilde{R} = 0.5$

It can be observed from the above figures that temperature rise with the decreasing values of \hat{K} .

4.3 Validation

In this section a comparison of the Nu values calculated from the present study for clear passage with the literature values [21] are given. Table 4.5 show the comparison for $\tilde{R} = 0.25$ and $\tilde{R} = 0.5$ respectively where \hat{K} is considered to be infinity.

Table 4.5: Validation with literature for $\hat{K} = \infty$

\tilde{R}	α	Nu		% change in Nu
		Calculated	Literature	
0.25	0.524	3.3493	3.6491	0.6
	0.262	3.6548	3.6523	0.068
	0.175	3.6976	3.6919	0.15
	0.131	3.6881	3.5791	0.24
0.5	0.524	3.0739	3.0727	0.039
	0.262	3.6169	3.6149	0.055
	0.175	4.0713	4.0684	0.071
	0.131	4.3782	4.3742	0.091

It can be seen from the tables that percentage change in Nu is within 1% which shows that the procedure adopted in this study is valid and the results obtained are compatible with literature.

Chapter 5

Conclusion and Future Work

In the present study we have carried out the fluid flow and heat transfer analysis of the Newtonian fluid flowing through the annular sector duct filled with Darcy-Brinkman porous medium. The problem is modeled subject to the H1 boundary condition applied at the inner surface of the heat transferring walls. The heat transferring surfaces are taken as isothermal. Results are presented for bulk mean velocity, bulk mean temperature, fRe and Nu for both the clear passage and the porous medium. Furthermore, the effect of sector length, sector angle and permeability of the fluid on the flow and heat transfer are discussed.

5.1 Conclusion

The summary of the conclusions made are as under.

- Bulk velocity is decreased and fRe is increased when varying only permeability. Same trend prevails for both values of \tilde{R} .
- Sector angle has mixed effect on bulk velocity and fRe .
- Bulk temperature and Nu number are increased but increase in Nu number is lesser than the increase in fRe for different values of \hat{K} .
- The effect of sector angle is non-monotonic on the T_b and Nu .

5.2 Future Work

We can extend the study in the following directions.

- The above trend suggests a presence of an optimal geometry for which heat transfer rate is maximum which can be an interesting further extension of this thesis.
- Conduction effect through the heated walls can be considered to make the problem realistic.

Bibliography

- [1] F. P. Incropera, D. P. DeWitt, T. Bergman, and A. Lavine. *Fundamentals of Heat and Mass Transfer*. 6 edition.
- [2] K. S. Syed, M. Iqbal, and N. A. Mir. Convective heat transfer in the thermal entrance region of finned double-pipe. *Heat Mass Transfer*, 43:449–457, 2007.
- [3] M. J. Lin, Q. W. Wang, and W. Q. Tao. Developing laminar flow and heat transfer in annular-sector ducts. *Heat Transfer Engineering*, 21(2):53–61, 2000.
- [4] Z. Y. Li, T. C. Hung, and W. Q. Tao. Numerical simulation of fully developed turbulent flow and heat transfer in annular sector duct. *Heat and Mass Transfer*, 38:369–377, 2002.
- [5] K. S. Syed, Z. Iqbal, and M. Ishaq. Optimal configuration of finned annulus in a double pipe with fully developed laminar flow. *Applied Thermal Engineering*, 31:1435–1446, 2011.
- [6] M. Kaviany. Laminar flow through a porous channel bounded by isothermal parallel plates. *International Journal Heat Mass Transfer*, 28(4):851–858, 1985.
- [7] H. J. Sung, S. Y. Kim, and J. M. Hyun. Forced convection from an isolated heat source in a channel with porous medium. *International Journal Heat and Fluid Flow*, 16:527–535, 1995.
- [8] I. Kurtbas and N. Celik. Experimental investigation of forced and mixed convection heat transfer in a foam-filled in a horizontal rectangular channel. *International Journal of Heat and Mass Transfer*, 52:1313–1325, 2009.
- [9] K. Hooman, H. Gurgenci, and A. A. Merrikh. Heat transfer and entropy generation optimization of forced convection in porous-saturated ducts of rectangular cross-section. *International Journal of Heat and Mass Transfer*, 50:2051–2059, 2007.

-
- [10] C. Y. Wang. Analytical solution for forced convection in a semi-circular channel filled with a porous medium. *Transport Porous Medium*, 73:369–378, 2008.
- [11] C. Y. Wang. Flow and heat transfer through a polygonal duct filled with a porous medium. *Transport Porous Medium*, 90:321–332, 2011.
- [12] D. Poulikakos and M. Kazmierczak. Forced convection in a duct partially filled with a porous material. *Journal of Heat Transfer*, 109(3):653–662, 1987.
- [13] A. Nakayama, H. Koyama, and F. Kuwahara. An analysis on forced convection in a channel filled with a brinkman-darcy porous medium: Exact and approximate solutions. *Wärme- und Stoffübertragung*, 23:291–295, 1988.
- [14] M. Hajipour and A. M. Dehkordi. Analysis of nanofluid heat transfer in parallel-plate vertical channels partially filled with porous medium. *International Journal of Thermal Sciences*, 55:103–113, 2012.
- [15] P. X. Jiang, G. S. Si, M. Li, and Z. P. Ren. Experimental and numerical investigation of forced convection heat transfer of air in non-sintered porous media. *Experimental Thermal and Fluid Science*, 28:545–555, 2004.
- [16] A. Haji-Sheikh and K. Vafai. Analysis of flow and heat transfer in porous media imbedded inside various-shaped ducts. *International Journal of Heat and Mass Transfer*, 47:1889–1905, 2004.
- [17] Y. P. Du, Z. G. Qu, C. Y. Zhao, and W. Q. Tao. Numerical study of conjugated heat transfer in metal foam filled double-pipe. *International Journal of Heat and Mass Transfer*, 53:4899–4907, 2010.
- [18] J. M. McDonough. *Lectures in Elementary Fluid Dynamics*. 2009.
- [19] Jr. J. D. Anderson. *Computational Fluid Dynamics*. McGraw Hill, 1995.
- [20] R. K. Shah and A. L. London. *Laminar Flow Forced Convection in Ducts*. Academic Press, London, 1978.
- [21] K. S. Syed. *A Simulation of Fluid Flow Through the Double Pipe Heat Exchanger*. PhD thesis, Department of Mathematics, University of Bradford, U. K., 1997.